UNIVERSITY *of* York

This is a repository copy of *Rapid and efficient adsorption of methylene blue dye from aqueous solution by hierarchically porous, activated starbons®:Mechanism and porosity dependence*.

White Rose Research Online URL for this paper:
https://eprints.whiterose.ac.uk/189132/

Version: Published Version

Article:

White Rose
university consortium
Universities of Leeds, Sheffield & York

eprints@whiterose.ac.uk
https://eprints.whiterose.ac.uk/

Research Paper

Rapid and efficient adsorption of methylene blue dye from aqueous solution by hierarchically porous, activated starbons®: Mechanism and porosity dependence

Han Li , Vitaliy L. Budarin , James H. Clark , Michael North [*], Xiao Wu

Green Chemistry Centre of Excellence, Department of Chemistry, University of York, York Y10 5DD, UK

HIGHLIGHTS

- Methylene blue adsorption from aqueous solution onto biomass derived carbon.
- Starch derived hierarchically porous carbon adsorbent (Starbon).
- Rapid adsorption which is reversible by pH swing allowing the Starbon to be reused.
- Adsorption capacity correlates to the BET surface area of the Starbon material.
- Adsorption capacity correlates to the micropore volume of the Starbon material.

GRAPHICAL ABSTRACT
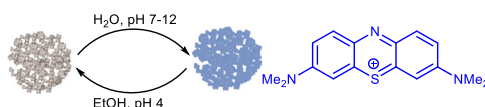
ABSTRACT

Hierarchically porous activated Starbons® derived from starch are found to make excellent adsorbents for methylene blue, even in the presence of other dyes and inorganic salts, highlighting their potential to be used in water purification. The optimal material (S950C90) has a methylene blue adsorption capacity (891 mg g^{-1}) almost nine times higher than that of unactivated S800 and four times higher than that of commercial activated carbon at 298 K. The adsorption of methylene blue onto optimal materials (S950C90 and S800K4) reaches equilibrium within 5 min. Adsorption data for all the adsorbents show a good fit to the Freundlich isotherm which allows the Gibbs free energies of adsorption to be calculated. The adsorption capacities increase as the pH of the methylene blue solution increases, allowing the dye to be desorbed by treatment with acidic ethanol and the Starbon® materials reused. Porosimetry and SEM-EDX imaging indicate that methylene blue adsorbs throughout the surface and completely fills all the micropores in the Starbon® adsorbent. The methylene blue adsorption capacities show excellent correlations with both the BET surface areas and the micropore volumes of the materials.

1. Statement of Environmental Implication

Methylene blue (MB) is toxic; environmentally persistent; non-biodegradable and stable to light, heat, water and oxidation. It is also the most widely used basic and cationic dye. Hence, release of MB into watercourses poses a significant hazard to aquatic life and to animals

---

further up the food chain including humans. MB is also a widely used model for other hazardous organic contaminants in water. Herein we show that starch derived, hierarchically porous carbons (activated Starbons®) have excellent adsorbent properties (high capacity, rapid rate of adsorption and dye release by pH-swing) for MB, making them applicable for purification of contaminated water.

2. Introduction

Dyes and pigments are widely used in areas including: leather tanning; printing; and production of textiles, paper, rubber, plastics, food and cosmetics (Sokolowska-Gajda et al., 1996; Kabdasli et al., 1999; Wrobel et al., 2001; Bhatnagar and Jain, 2005; Bensalah et al., 2009). Annual production of dyes and pigments is over 700,000 tonnes, of which 2–15% is lost in the effluent during a dyeing process (Robinson et al., 2001; Lee et al., 2006; Tan et al., 2007; Muhammad and Muhammad, 2007). Dyeing has a visible effect on water quality as water colouration occurs at dye concentrations below 1 ppm (Banat et al., 1996; Al-Degs et al., 2000; Wong et al., 2004; Forgacs et al., 2004). Many synthetic dyes are toxic, environmentally persistent and non-biodegradable (Dogan et al., 2007). Hence, the release of dye containing waste streams into watercourses can pose a significant hazard to aquatic life and to animals further up the food chain including humans (Walsh and Bahner, 1980; Ramakrishna and Viraraghavan, 1997; O'Neill et al., 1999; Bhattacharyya and Sharma, 2004). Dyes tend to be stable to light, heat, water and oxidation, making treatment of contaminated waste streams a significant challenge (Sun and Yang, 2003; Golob and Ojstrsek, 2005; Singh and Arora, 2011).

Various techniques have been explored to remove dyes from wastewater (Manohara et al., 2021) including biological (Ali, 2010) or chemical (Katheresan et al., 2018) treatments and physical processes (Singh et al., 2018). Biological methods include bioremediation of dyes by microorganisms such as algae, bacteria or fungi, or by isolated enzymes and can be based on aerobic or anaerobic processes. These methods are inexpensive and non-toxic, but the growth of the microorganism needs a suitable environment (Singh et al., 2022). Chemical methods include oxidation process (such as Fenton reactions and ozonolysis), chemisorption and electrochemical destruction. These methods are often more efficient than biological processes, but they require specific equipment and chemical reagents and generate toxic secondary pollutions (Katheresan et al., 2018; Saravanan et al., 2021). Physical methods including physisorption, screening, coagulation, ion exchange, irradiation and membrane-based technologies are usually used before the other two methods due to their simplicity. They require the least amount of additional chemicals, are easily regenerated and have high dye removal efficiency (Ahmed et al., 2021). Physical adsorption (physisorption) and chemical adsorption (chemisorption) can be distinguished based on the interaction energy between the adsorbent and the adsorbed species. Physisorption is characterised by weak van der Waals, dipole–dipole, polare interactions, or hydrogen bonding between the adsorbent and adsorbate and thus is usually reversible and nonselective. In contrast, chemisorption occurs via formation of strong bonds (ionic or covalent), which is usually irreversible and selective (Mashkoor and Nasar, 2020).

Amongst these techniques, adsorption (especially physisorption) is preferred due to its ease of operation, low energy requirement, insensitivity to toxic pollutants and high efficiency (Yagub et al., 2014). It has the ability to remove almost any type of dye without the production of secondary pollutants (Kyzas and Matis, 2015; De Gisi et al., 2016; Ngulube et al., 2017). Many adsorbents including zeolites (Rad and Anbia, 2021), silica-based materials (Alam et al., 2021), metal–organic frameworks (Gao et al., 2019), polymeric materials (Subhan et al., 2022), clay-organic composites (Ozola-Davidane et al., 2021) and carbons (activated carbon, biochar, graphitic carbon, carbon xerogels, carbon nanoparticles) (Santoso et al., 2020) have been extensively investigated for dye adsorption. Most of these adsorbents can remove

pollutants from water, but suffer from drawbacks including low efficiency, high cost and poor reusability. (Saxena et al., 2020; Santoso et al., 2020).

In addition to the above requirements, a potential adsorbent for the removal of dyes from wastewater should also be economically viable and readily available (Katheresan et al., 2018). Commercial activated carbons, derived from coal, have been used as adsorbents for the treatment of dye waste in the textiles industry due to their large surface areas, microporous structure, thermal stability and low acid/base reactivity. However, high costs limit their large scale use (Yagub et al., 2014; Montoya-Suarez et al., 2016; Tan et al., 2017). Hence, a wide variety of low-cost materials including natural resources (e.g. wood, bark, clays, zeolites), agricultural wastes (e.g. sawdust, leaves, fibers, fruits peels, seeds), industrial by-products (e.g. sludge, fly ash, red mud), biomass (e. g. chitin, seaweed, fungi, yeast, algal waste, cellulosic materials, chitosan) and biomass derived activated carbons have been explored for this application (Rafatullah et al., 2010; Srinivasan and Viraraghavan, 2010; Solangi et al. 2021; Adegoke and Bello, 2015; De Gisi et al., 2016; Rahman et al., 2021).

Numerous studies on utilizing activated carbons derived from biomass for dye adsorption have been reported in recent years (Ani et al., 2020; Wong et al., 2018; Hassan and Carr, 2021). Biomass is diverse, abundant, renewable and sustainable and the activation process is relatively simple due to the high reactivity of the biomass. Thus, utilizing activated carbon obtained from biomass as an adsorbent can provide an economic and sustainable replacement for non-renewable coal-based activated carbon, whilst minimizing the impact to the environment (González-García, 2018). However, activated carbons produced from biomass are still limited in practical use as their pore sizes are far from optimal, resulting in large volumes of adsorbent being required (Singh and Rawat, 1994; Wong et al., 2018). In addition, it is difficult to achieve high uptake and a high rate of adsorption simultaneously due to the low accessibility of microporous surfaces and the large diffusion distance in the unimodal pores of most activated carbons (Qi et al., 2019). The heterogeneous texture of the biomass, the activation method and the activation conditions all affect the surface chemistry and the development of the pore structure in the resulting activated carbon (Wang et al., 2021; Gayathiri et al., 2022). Therefore, to overcome the limitations of low adsorption efficiency and slow adsorption rate, selection of appropriate biomass precursors and activation methods and optimization of the activation conditions are key factors for reproducibly obtaining activated carbons in high yield and of appropriate quality for industrial wastewater treatment.

Methylene blue (**1**) is the most widely used basic and cationic dye in textiles, printing, biology and chemistry (Khan et al., 2022). As a large heterocyclic aromatic compound (Fig. 1) it is used extensively to evaluate the structure and adsorption capacity of activated carbons, as the available surface of an adsorbent for a large molecule such as **1** is limited due to the molecular sieving effect (Barton, 1987). In previous work, it has been shown that predominantly mesoporous carbons (Starbons®) derived from starch or alginic acid have higher adsorption capacities and faster adsorption rates for dye **1** than those of conventional, microporous activated carbon (Parker et al., 2012).

Recently, we showed that mesoporous Starbons® could be activated by treatment with potassium hydroxide, carbon dioxide or oxygen to produce hierarchically porous materials with superior carbon dioxide adsorption capacities to either mesoporous Starbons® or microporous
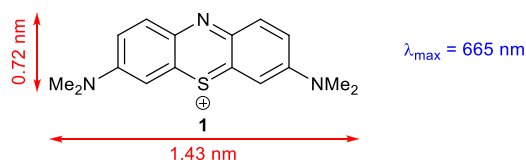
Fig. 1. Structure and key parameters of methylene blue cation **1**.

activated carbon (Li et al., 2022). The aim of the current work was to investigate if the hierarchically porous nature of activated Starbons® would also be beneficial for the adsorption of methylene blue and other dyes. The large surface areas produced by the presence of micropores and small mesopores were expected to provide sites for dye adsorption, whilst the presence of larger mesopores and macropores should facilitate rapid dye diffusion, and the macropores would act as reservoirs to minimise diffusion distances (Chen et al., 2015; Albadarin et al., 2017; Qi et al., 2019; Zhang et al., 2020). However, dye **1** is a much larger molecule than carbon dioxide (which has a kinetic diameter of just 0.33 nm (Rehman and Park, 2019)), so the optimal materials for adsorption of carbon dioxide might not be optimal for the adsorption of dye **1**. In this manuscript we show that hierarchically porous Starbons® do indeed make excellent adsorbents for methylene blue **1**.

3. Results and discussion

3.1. Methylene blue adsorption and desorption studies

3.1.1. Synthesis and characterisation of adsorbents

Eleven carbon-based materials were selected for this investigation and their textural properties are detailed in Table 1. Commercial activated carbon (AC) provided a predominantly microporous control sample (Martin et al., 2003). The other ten materials were all prepared from starch as previously reported (Li et al., 2022) and outlined in Fig. 2. S800 is unactivated Starbon® produced by pyrolysis of expanded starch at 800 °C. This provided a predominantly mesoporous control sample.[1] S800K1–K5 are potassium hydroxide activated Starbons® prepared at 800 °C using 1–5 equivalents (g/g) of potassium hydroxide. S950C30–90 are carbon dioxide activated Starbons® prepared by treatment of S800 with carbon dioxide at a maximum temperature of 950 °C for 30, 60 or 90 min. S750O0 is an oxygen activated Starbon® prepared by heating S800 to 750 °C under a gas flow comprising 2% oxygen and 98% nitrogen. The nine activated Starbons® in this set of materials had a wide range of surface areas and porosities (Table 1), allowing the impact of these parameters on their methylene blue adsorptions to be investigated.

3.1.2. Methylene blue adsorption capacities and removal efficiencies at 298 K

The adsorption of methylene blue by the carbon-based materials was studied by UV-Vis spectrophotometry, monitoring the decrease in adsorption at 665 nm of an aqueous solution of **1** of known initial concentration and converting the adsorption to concentration using a calibration curve (data in supporting information). This was used to calculate: the quantity of dye **1** adsorbed at time t (q_t, mg g^{-1}), the adsorption capacity of dye **1** at equilibrium (q_e, mg g^{-1}), the percentage removal of dye **1** at time t (R_t, %) and the removal efficiency of dye **1** (R_e, %) according to equations 1–4 (Fu et al., 2016) where C_0 (mg L^{-1}), C_t (mg L^{-1}) and C_e (mg L^{-1}) are the initial, at time t, and equilibrium concentrations of **1** respectively; V (L) is the volume of solution; and m (g) is the mass of adsorbent.

1: $q_t = (C_0 - C_t)V/m$.
2: $q_e = (C_0 - C_e)V/m$.
3: $R_t = 100(C_0 - C_t)/ C_0$.
4: $R_e = 100(C_0 - C_e)/C_0$.

The equilibrium adsorption capacities of the adsorbents at various initial dye **1** concentrations at 298 K were determined in triplicate after contact times of 24 h and the average values are presented in Table 2 (for graphical representations of this data see supporting information). The adsorption capacities (q_e) initially increased as the dye

concentration increased indicating that there were sufficient adsorption sites for dye **1** on the adsorbents at low concentrations. Then, the saturated adsorption capacities were obtained at higher concentrations of dye **1**. All the Starbons® exhibited excellent removal efficiencies (R_e) towards dye **1** at low initial methylene blue concentrations (close to 100%). As the initial concentration of the dye **1** solution increased, the removal efficiencies decreased as the absorbents reached their saturated adsorption capacities and all adsorption sites became saturated with methylene blue molecules.

Compared to S800 and to activated carbon, the activated Starbons® all have much higher saturated adsorption capacities for dye **1**. S950C90 has the largest saturated adsorption capacity (891 ± 43 mg g^{-1}) and a removal efficiency of (74 ± 4%) at a dye **1** concentration of 600 mg L^{-1}. This saturated adsorption capacity is almost nine times higher than that of S800 (106 ± 8 mg g^{-1}) and four times higher than that of activated carbon (231 ± 6 mg g^{-1}). The exceptionally high saturated adsorption capacity of S950C90 can be attributed to its well-developed hierarchical porous structure (Qi et al., 2019) as it has the highest surface area, micropore volume, mesopore volume and total pore volume of any of the materials in Table 1. Its micropores provide adsorption sites for dye **1**; whilst the abundant meso- and macropores provide spaces to reduce the steric hindrance between adsorbed dye molecules and to facilitate the diffusion of dye molecules into the adsorbent (Xiao et al., 2006; Chang et al., 2017; Zhang et al., 2020). The high adsorption capacities and removal efficiencies for dye **1** by activated Starbons® show the potential of these materials in practical applications involving decolouration of wastewater.

3.1.3. Temperature dependence of methylene blue adsorption capacities and removal efficiencies

The effect of temperature on the equilibrium capacities and removal efficiencies of the two best performing materials (S800K4 and S950C90) was studied between 298 and 318 K at various concentrations of dye **1** (see supporting information). The adsorption capacities of the materials increased as the initial concentration of **1** increased at each temperature, though the saturated adsorption capacities were independent of temperature over the temperature range studied. In addition, more than 95% removal efficiency of dye **1** could be achieved by both Starbons® at initial dye concentrations of 300 and 400 mg L^{-1} throughout the range of temperatures investigated. This highlights the high efficiency of methylene blue adsorption onto these two adsorbents even at high initial dye concentrations compared to the other samples detailed in Table 2. The results suggest that S800K4 and S950C90 have surface areas and micropore volumes which optimise the number of adsorption sites which are accessible to dye **1**. At all temperatures, at the higher initial dye concentrations (500–700 mg L^{-1}), the adsorption capacities and removal efficiencies of S950C90 were higher than those of S800K4. The highest saturated adsorption capacity onto S950C90 was 919 ± 15 mg g^{-1}.

3.1.4. Fitting of methylene blue adsorption data to isotherm models

To investigate the nature of the equilibrium adsorptions, the experimental equilibrium adsorption data (q_e and C_e) was fitted to the Langmuir, Freundlich and Temkin isotherm models (Al-Ghouti and Da'ana, 2020). The resulting best fit plots, optimised parameters and correlation coefficients are given in the supporting information. The best fit to the data across all eleven materials was obtained using the Freundlich isotherm as judged by the correlation coefficients (R^2) which were greater than 0.8 in every case (Table 3). This indicates that the adsorption process is multilayer and non-ideal with adsorption sites distributed non-uniformly on the heterogeneous surface of the material with varying heats of adsorption and adsorption affinities (Al-Ghouti and Da'ana, 2020). The adsorption driving force and the surface heterogeneity can be evaluated in the Freundlich model, by the value of 1/n which represents the adsorption affinity or the degree of the surface heterogeneity (Chaari et al., 2015). These values were all less than 0.5,

---

[1] This S800 material differs from that reported in (Parker et al., 2012) as it was prepared by the greener freeze-drying method rather than the solvent exchange method.

Table 1
BET-surface areas and pore volumes for Starbon® materials.

Entry	Material	S_{BET} (m^2 g^{-1})	V_{micro} (cm^3 g^{-1})[a,b]	$V_{ultramicro}$ (cm^3 g^{-1})[a]	V_{meso} (cm^3 g^{-1})[c]	V_{total} (cm^3 g^{-1})[d]	micropore (%)[e]	ultramicropore (%)
1	AC	812	0.34	0.21	0.40	0.74	45.9	28.4
2	S800	619	0.24	0.19	0.35	0.59	40.7	32.2
3	S800K1	1214	0.48	0.32	0.58	1.06	45.3	30.2
4	S800K2	1294	0.49	0.39	0.10	0.59	83.1	66.1
5	S800K3	1633	0.62	0.45	0.14	0.77	80.5	58.4
6	S800K4	2299	0.91	0.46	0.07	0.98	92.9	46.9
7	S800K5	2452	1.00	0.57	0.09	1.09	92.7	52.3
8	S950C30	1618	0.64	0.46	0.27	0.94	68.1	48.9
9	S950C60	2180	0.89	0.53	0.41	1.32	67.4	40.2
10	S950C90	2457	1.04	0.56	0.59	1.64	63.4	34.1
11	S750O0	1100	0.43	0.33	0.14	0.58	74.1	56.9

[a] Calculated based on the HK model.
[b] Includes the ultramicropore volume.
[c] Calculated based on the BJH model.
[d] Calculated based on the HK model at $P/P_0 = 0.99$.
[e] Includes the ultramicropore %.
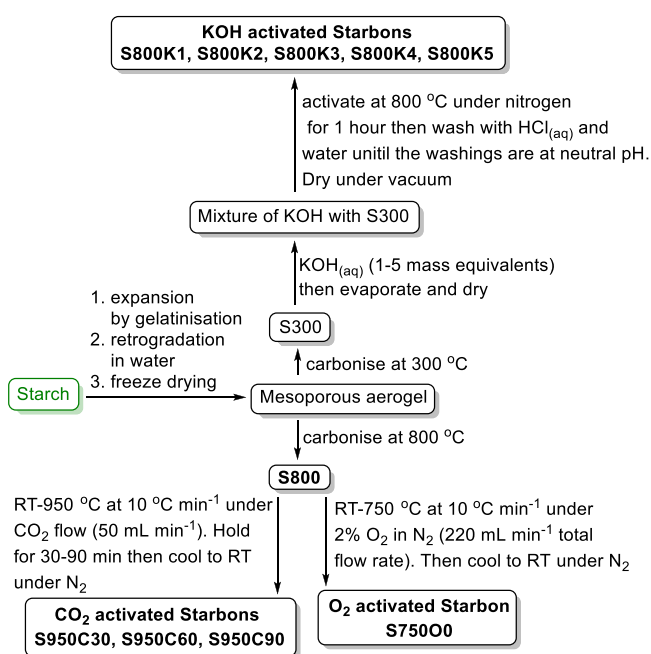
Fig. 2. Routes used to prepare Starbon® materials. Materials shown in bold are those used in this work.

indicating that the adsorption of dye **1** occurred easily.

The Freundlich isotherm constants (K_F) are related to the equilibrium adsorption constants (K_{ads}) as shown in equation 5 and hence allow the Gibbs free energy of adsorption (ΔG_{ads}) to be calculated (Zhang et al., 2020). At 298 K, all of the materials had ΔG_{ads} values for the adsorption of dye **1** between -23.7 and -31.4 kJ mol^{-1} as shown in Table 3. These negative values for the Gibbs free energy changes confirm the spontaneous nature of the adsorption process. The least negative value (-23.7 kJ mol^{-1}) was obtained for the predominantly mesoporous S800. The two most negative values at 298 K (-30.7 and -31.4 kJ mol^{-1}), corresponding to adsorption of dye **1** being most favourable, were obtained for S950C90 and S800K4 respectively, the two materials which were experimentally found to have the highest adsorption capacities for dye **1** (Table 2). At higher temperatures, the Gibbs free energies of adsorption became more negative, decreasing to -32.6 kJ mol^{-1} at 318 K for S800K4 and to -33.7 kJ mol^{-1} at 318 K for S950C90. Thus, the adsorption of methylene blue onto activated Starbons® is well represented by the Freundlich isotherm model and this allows thermodynamic parameters associated with the adsorption to be determined.

5: $K_{ads} = (K_F \rho / 1000)[(10^6/\rho)^{(1-(1/n))}]$.
where ρ is the density of water (taken as 1.0 g mL^{-1}).

3.1.5. Kinetics of Methylene blue adsorption

The kinetics of methylene blue adsorption were investigated and the results in Fig. 3 show that dye **1** was initially rapidly adsorbed onto all the materials and adsorption equilibria ($q_{e\text{-}exp}$) were reached within a maximum of three hours. Due to the low surface coverage in the early stages of adsorption, dye molecules could rapidly occupy vacant adsorption sites. As the dye adsorption progressed and approached equilibrium, the number of available adsorption positions reduced and dye **1** already adsorbed on the adsorbent caused steric hindrance and electrostatic repulsion for other approaching dye molecules (Albadarin et al., 2017). Adsorption of dye **1** onto potassium hydroxide, carbon dioxide and oxygen activated Starbons® and onto activated carbon (Fig. 3a,c–k) was more rapid than adsorption onto unactivated S800 (Fig. 3b). Most of the methylene blue was adsorbed in the first thirty minutes and for S800K4 (Fig. 3f) and S950C90 (Fig. 3j), the times required for the adsorption to reach equilibrium were as short as five minutes.

The experimental adsorption data were fitted to pseudo-second order (Albadarin et al., 2017) and Elovich (Fan et al., 2017) models. The experimental adsorption data and fitting plots are shown in Fig. 3 and selected adsorption parameters obtained from the pseudo-second order model are given in Table 4, with full data for both models provided in the supporting information. Both the pseudo- second order (equation 6) and Elovich kinetic models gave good fits to the experimental data (see supporting information) though the pseudo-second order model had higher correlation coefficient values (close to unity) and gave q_e values ($q_{e\text{-}cal}$) that were consistent with the experimental data ($q_{e\text{-}exp}$) as shown in Table 4. Thus, the pseudo-second order model was used to analyse the data. This model assumes that the adsorption process includes diffusion of the external liquid film, surface adsorption and intra-particle diffusion processes, and that the adsorption rate is determined by the number of unoccupied adsorption sites on the adsorbent surface (Albadarin et al., 2017). The h_2 term in equation 6 indicates the initial adsorption rate whilst k_2 is the rate constant at equilibrium. The data in Table 4 show that S950C90 has an exceptionally high h_2 value of 34,770 which is an order of magnitude higher than that of S800K4 (8065) whose h_2 value is itself one to three orders of magnitude greater than that of any other sample at the same initial dye concentration (400 mg L^{-1}). Activated Starbon® S800K2 has a h_2 value 3.7 times that of the corresponding unactivated Starbon® (S800) at the same initial dye concentration of 100 mg L^{-1}.

The h_2 values of S800K4 and S950C90 are far higher than those reported for other materials at the same initial dye concentrations such as: clays (1.5–5.0 mg g^{-1} min^{-1}) (Gürses et al., 2006); a biosorbent prepared

Table 2
Adsorption capacities (q_e) and removal efficiencies (R_e) for adsorption of **1**.

Material	1 C_0 (mg L^{-1})	q_e (mg g^{-1})	R_e (%)	1 C_0 (mg L^{-1})	q_e (mg g^{-1})	R_e (%)
AC	100	184.5 ± 9.0	92.3 ± 4.5	200	230.5 ± 6.3	57.6 ± 1.6
	150	218.4 ± 3.4	72.8 ± 1.1	250	225.1 ± 11.8	45.0 ± 2.4
S800	25	49.3 ± 0.3	98.7 ± 0.6	80	105.8 ± 3.2	66.1 ± 2.0
	50	93.9 ± 4.0	93.9 ± 4	90	105.9 ± 7.7	58.8 ± 4.3
	70	106.5 ± 4.0	76.1 ± 2.8	100	99.7 ± 6.5	49.8 ± 3.2
S800K1	100	197.6 ± 0.9	98.8 ± 0.43	400	340.5 ± 9.2	42.6 ± 1.2
	200	346.6 ± 2.7	86.6 ± 0.7	500	345.4 ± 21.8	34.5 ± 2.1
	300	347.3 ± 5.0	57.9 ± 0.8			
S800K2	50	98.9 ± 0.4	98.8 ± 0.4	300	238.7 ± 15.0	39.8 ± 2.5
	100	192.3 ± 4.6	96.2 ± 2.3	400	244.7 ± 9.7	30.6 ± 1.2
	200	248.3 ± 6.0	62.1 ± 1.5			
S800K3	100	191.2 ± 3.3	95.6 ± 1.6	400	483.2 ± 21.3	60.4 ± 5.2
	200	360.3 ± 10.3	90.1 ± 2.6	500	489.2 ± 36.6	48.9 ± 3.7
	300	491.1 ± 23.7	81.9 ± 4.0			
S800K4	300	597.9 ± 0.7	99.7 ± 0.1	600	811.0 ± 36.9	67.6 ± 3.1
	400	771.8 ± 16.5	96.5 ± 2.1	700	817.0 ± 46	58.4 ± 4
	500	787.2 ± 22.7	78.7 ± 2.3			
S800K5	200	398.4 ± 0.9	99.6 ± 0.2	400	638.9 ± 21.4	82.4 ± 2.7
	300	557.3 ± 24	92.9 ± 4	500	629.0 ± 3.1	62.9 ± 0.3
S950C30	200	394.4 ± 0.8	98.6 ± 0.2	500	494.8 ± 37.2	49.5 ± 3.7
	300	511.0 ± 31.2	85.2 ± 5.2	600	515.9 ± 5.3	43.0 ± 0.4
	400	510.5 ± 24.8	63.8 ± 3.1			
S950C60	300	579.2 ± 8	96.5 ± 1.3	500	726.1 ± 33.1	72.6 ± 3.3
	400	655.9 ± 6.1	82.0 ± 0.8	600	725.8 ± 13.4	60.5 ± 1.1
S950C90	300	597.9 ± 1.4	99.7 ± 0.2	500	825.9 ± 38.7	82.6 ± 3.9
	400	782.5 ± 18.4	97.8 ± 2.3	600	891.0 ± 43.1	74.3 ± 3.6
S750O0	100	196.6 ± 1.0	98.3 ± 0.5	200	308.9 ± 1.9	77.2 ± 0.5
	125	245.9 ± 2.2	98.4 ± 0.9	250	328.4 ± 24.1	65.7 ± 4.8
	150	289.1 ± 9.8	96.4 ± 3.3			

Table 3
Freundlich adsorption isotherm parameters for the adsorption of dye **1**.

Sample	T (K)	1/n	K_F (mg g^{-1} (L mg^{-1})$^{1/n}$)	ΔG_{ads} (kJ mol^{-1})	R^2
AC	298	0.0737	162.0	-27.2	0.91
S800	298	0.1147	70.79	-23.7	0.83
S800K1	298	0.0756	234.6	-28.1	0.86
S800K2	298	0.0953	150.9	-26.3	0.95
S800K3	298	0.1766	199.6	-24.2	0.86
S800K4	298	0.0493	628.9	-31.4	0.89
	303	0.0661	591.8	-31.2	0.97
	308	0.0613	601.0	-31.9	0.91
	318	0.0666	566.4	-32.6	0.94
S800K5	298	0.0879	421.4	-29.1	0.93
S950C30	298	0.0492	392.7	-30.2	0.80
S950C60	298	0.0771	482.1	-29.8	0.95
S950C90	298	0.0686	627.9	-30.7	0.92
	308	0.0612	632.3	-32.0	0.96
	318	0.0500	687.5	-33.7	0.94
S750O0	298	0.0930	219.8	-27.3	0.81

represented by a pseudo-second order model and this shows that the materials with the highest saturated adsorption capacities also have the highest rates of adsorption.

3.1.6. Effect of solution pH on methylene blue adsorption by S950C90

Both the methylene blue and the surface charge of the Starbon® could be affected by the pH of the dye **1** solution (Hu et al., 2018). The solution pH which produces a surface charge (Zeta potential) of zero on the adsorbent is referred to as pH$_{zpc}$ (Zhang et al., 2020). The best performing Starbon® material (S950C90) was found to have a pH$_{zpc}$ of 5 (Fig. 4a). Thus, at pH values below 5 the surface of S950C90 will be positively charged whilst at pH values above 5, its surface will be negatively charged. Therefore, the effect of the pH of the methylene blue solution on the saturated adsorption capacity and removal efficiency of dye **1** by S950C90 was investigated. Fig. 4b shows that the solution pH does influence the adsorption of dye **1** by S950C90. The saturated adsorption capacity and removal efficiency increased from (819 ± 36 mg g^{-1}) and (82 ± 4%) respectively at pH 4 to (937 ± 20 mg g^{-1}) and (94 ± 2%) at pH 9. Above pH 9 there was no further increase in the saturated adsorption capacity or removal efficiency. These results indicate that there is an electrostatic component to the adsorption of dye **1** onto S950C90 with a surface with negative Zeta potential being favourable for the adsorption of positively charged dye **1** (Hu et al., 2018).

3.1.7. Desorption of methylene blue from S950C90 and recyclability of the adsorbent

The Zeta potential data also suggested that desorption of dye **1** from S950C90 would be favoured at low pH's which would allow the reuse of the adsorbent. It was found that desorption could be achieved by treatment of the adsorbed dye with a solution of ethanol and ethanoic acid (20/1, v/v) and was facilitated by ultrasonication of the suspension. Previous work (Tang et al., 2021) using this solvent system for methylene blue desorption indicated that desorption occurs due to competition between protons from ethanoic acid and dye **1** cations, whilst ethanol provides similar polar forces to the dye molecules to those present when the dye is adsorbed on the Starbon® material.

The recyclability of S950C90 over four cycles of dye **1** adsorption and desorption (at 298 K and C_0 =500 mg L^{-1}) is shown in Fig. 5. The first cycle saturated adsorption capacity was 793 mg g^{-1} and the first desorption removed 756 mg g^{-1} or 95% of the adsorbed dye. The second to fourth cycles also desorbed 97–99% of the adsorbed dye, though the saturated adsorption capacities decreased over these three cycles to 660, 597 and 586 mg g^{-1} (based on the initial mass of S950C90 used), due to unremoved dye **1** and water; and to unavoidable handling losses. The data show that S950C90 is a highly recyclable adsorbent for methylene blue dye.

from agrobacterium fabrum (0.9–22 mg g^{-1} min^{-1}) (Sharma et al., 2018); carbon dioxide activated spherical carbon prepared from sucrose (18–34 mg g^{-1} min^{-1}) (Bedin et al., 2018); potassium hydroxide activated carbon prepared from Date Press Cake (108–600 mg g^{-1} min^{-1}) (Heidarinejad et al., 2018) and hydrothermal, potassium hydroxide activated carbon prepared from coffee husk (19–278 mg g^{-1} min^{-1}) (Tran et al., 2021).

6: $q_t = h_2 t (1 + k_2 q_e t)^{-1}$ where $h_2 = k_2 q_e^2$.

The high h_2 values for S800K4 and S950C90 can be related to their optimal pore structure which facilitates the adsorption of dye molecules onto the surface sites as discussed above (Zhang et al., 2020). Hence the adsorption of methylene blue by activated Starbon® materials is well

Fig. 3. Variation of adsorption of dye **1** onto carbon-based materials with time at 298 K. Experimental data points are shown as squares, the best fit to the pseudo-second order kinetic model is indicated by the solid lines and the best fit to the Elovich kinetic model is indicated by the dashed lines.

Table 4
Experimental and pseudo-second order kinetic parameters for adsorption of **1**.

Material	C_0 (mg L^{-1})[a]	q_{e-exp} (mg g^{-1})	k_2 (g mg^{-1} min^{-1})	q_{e-calc} (mg g^{-1})	h_2 (mg g^{-1} min^{-1})	R^2
AC	100	194.9	0.0030	193.1	110.1	0.9999
S800	100	109.9	0.0006	111.5	7.8	0.9936
S800K1	400	324.3	0.0013	327.9	135.5	1.0000
S800K2	100	197.8	0.0007	201.6	28.7	0.9990
S800K2	400	140.5	0.0004	150.4	8.6	0.9955
S800K3	400	428.1	0.0006	427.4	113.5	0.9990
S800K4	400	765.3	0.0132	781.3	8065	0.9990
S800K5	400	604.3	0.0008	602.4	295.9	0.9990
S950C30	400	483.8	0.0005	485.4	124.4	0.9980
S950C60	400	748.7	0.0014	746.3	800.0	1.0000
S950C90	400	798.1	0.0543	799.9	34,770	1.0000
S750O0	100	194.9	0.0030	193.1	110.1	0.9990

[a] Only data at C_0 = 100 or 400 mg L^{-1} is included (with both concentrations given for S800K2) and the value reported is after a contact time of 3 h. Data for other initial concentrations are given in the supporting information.

3.2. Analysis of methylene blue adsorbed on starbons®

3.2.1. TGA-FTIR analysis

To understand the adsorption behaviour of dye **1**, the best performing adsorbent (S950C90) was pyrolysed under nitrogen from 20 to 625 °C in a thermogravimetric analyser coupled to a Fourier transform infrared spectrometer (TG-FTIR) with a heating rate of 10 °C min^{-1} and a hold time at 625 °C of 1 h, both before and after methylene blue adsorption (298 K and C_0 =500 mg L^{-1}). For comparison, methylene blue chloride was also pyrolysed under the same conditions. Due to the evaporation of water, mass losses of 16%, 16% and 2% are observed below 100 °C in the TGA curves of methylene blue chloride, S950C90, and S950C90 after adsorption of **1** (Fig. 6a) with corresponding peaks observed at temperatures below 100 °C by differential thermal gravimetry (DTG) (Fig. 6b).

Above 100 °C, S950C90 underwent only a 10% mass loss due to slight dehydration and decomposition. The FTIR spectrum of the off-gases (Fig. 6c) shows peaks corresponding to water (1700–1800 and 3300–3800 cm^{-1}) throughout the heat treatment, and to carbon dioxide (2350 and 667 cm^{-1}) enhancing gradually from 600 s which corresponds to a temperature of 120 °C. In contrast, methylene blue undergoes significant decomposition above 100 °C, resulting in a mass loss of 46% (Fig. 6a). Due to the existence of methylene blue within the pore structure of S950C90, the mass loss of S950C90 after adsorption of dye **1** increased to 30%. The FTIR spectra of the off-gases from thermal analysis of S950C90 after adsorption of dye **1** show the additional presence of ammonia (800–1200 cm^{-1}) and methane (2800–3100 cm^{-1}) at 1200–4000 s (corresponding to 220–625 °C) as shown in Fig. 6d–f. The hydrogen and nitrogen come from the decomposition of adsorbed methylene blue (see supporting information for FTIR spectra of the off-gases from heating just methylene blue). Due to the presence of hydrogen bonding and electrostatic interactions between the surface of S950C90 and methylene blue molecules, the decomposition temperatures of methylene blue adsorbed onto S950C90 (216 and 418 °C) were higher than those of pure methylene blue (214 and 297 °C) as shown in Fig. 6b. Based on the mass loss above 100 °C seen for methylene blue, S950C90 and methylene blue adsorbed onto S950C90, the adsorption capacity of S950C90 for dye **1** was calculated as 851 mg g^{-1} which compares well with the value of (826 ± 39) mg g^{-1} determined by UV–vis spectrophotometry (data in supporting information). Thus, the TGA-FTIR data both qualitatively and quantitatively confirmed the presence of methylene blue adsorbed within S950C90.
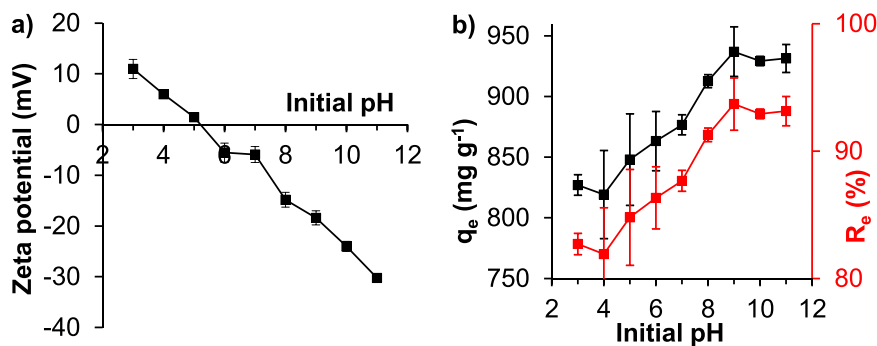
Fig. 4. Zeta potential (a) and saturated adsorption capacity and removal efficiency (b) of S950C90 as a function of the pH of the methylene blue solution. Triplicate experiments were conducted and error bars represent standard deviations.
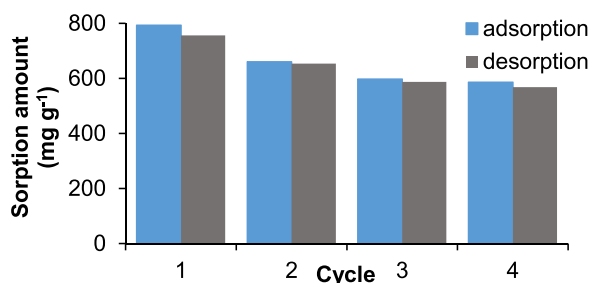
Fig. 5. Recyclability of S950C90 for methylene blue adsorption at 298 K. Saturated adsorption capacities are all calculated based on the amount of S950C90 used for cycle 1.

3.2.2. Combustion analysis and XPS

Based on the adsorption capacities of S950C90 and S800K4 for dye **1** at 298 K with an initial dye concentration of 500 mg L^{-1} (data in supporting information), the content of nitrogen and sulphur introduced into S950C90 and S800K4 after adsorption of dye **1** were calculated to be 5.9% and 4.5% respectively for S950C90 and 5.8% and 4.4% respectively for S800K4. The elemental compositions of S950C90, S800K4 and the corresponding materials after adsorption of dye **1** were determined by combustion analysis and the data are presented in Table 5. The increase in nitrogen and sulphur content after adsorption of dye **1** were 4.3% and 3.1% for S950C90 and 4.9% and 2.3% for S800K4, which are close to the calculated values.

The surface elemental composition of S950C90 and S800K4, before and after methylene blue adsorption was analysed by X-ray photoelectron spectroscopy (XPS). High-resolution C1s, N1s and O1s spectra of S950C90 and S800K4 after dye **1** adsorption are given in Fig. 7 and the corresponding wide-scan spectra (before and after dye **1** adsorption), along with a tabulation of the deconvoluted contributions to the high resolution C1s and O1s peaks are given in the supporting information.

The elemental compositions obtained by integrating the C1s, O1s and N1s peaks are given in Table 5. The presence of peaks corresponding to N1s and S2p in the spectra of S950C90 and S800K4 after adsorption of dye **1** indicates the presence of methylene blue on the surface of the materials. Deconvolution of the high resolution C1s peaks of S950C90 and S800K4 gave contributions at 286.6 ± 0.1, 288.3 ± 0.2 and 289.8 ± 0.3 eV corresponding to C–O or C–N; C═O; and O–C═O groups respectively (Plaza et al., 2013). After methylene blue adsorption, these peaks shifted to 286.1 ± 0.1, 287.8 and 289.2 eV which suggests an electrostatic attraction between the negative charged oxygen containing groups on the Starbon® and the positive charged dimethyliminium (═N$^+$Me$_2$) groups on methylene blue (Fu et al., 2016). Similarly, deconvolution of the O1s peaks of S950C90 and S800K4 gave contributions at 533.2, 535.4 and 538.0 ± 0.9 eV corresponding to C–O, O–C═O and C═O groups respectively. After methylene blue adsorption,

these peaks shifted to 532.7 ± 0.1, 534.4 ± 0.3 and 536.9 ± 0.2 eV, suggesting an interaction of the oxygen containing groups within the activated Starbons® with methylene blue (Li et al., 2020). Peak component intensity changes were also seen after adsorption of dye **1** onto S950C90 or S800K4. The concentration of C–N groups increased significantly by 4.2–7.1%, whilst the intensities of the peaks at 290.9 and 294.0 eV arising from π-π * transitions within the aromatic rings of S950C90 and S800K4 decreased after adsorption of dye **1**, suggesting π-π interactions between the aromatic rings of the Starbons® and the conjugated system of dye **1** (Zhang and Xu, 2014). Hence, the XPS data suggests that the adsorption of cationic methylene blue **1** onto S950C90 and S800K4 depends on both electrostatic and π-π interactions.

3.2.3. Porosimetry

To further verify the incorporation of dye **1** molecules into the porous structure of the Starbon® adsorbent, the nitrogen adsorption-desorption isotherms of S800K4 were measured at 77 K both before and after methylene blue adsorption. Fig. 8 shows that the initially highly microporous S800K4 was completely converted into a nonporous material after methylene blue adsorption as both the micropores and mesopores were filled by dye molecules.

3.2.4. SEM and EDS imaging

The surface morphology and element composition of S950C90 before and after dye **1** adsorption were also studied by SEM and EDS imaging (Novais et al., 2018) as shown in Fig. 9 (see supporting information for additional lower magnification images). Fig. 9 shows that there are fewer mesopores and macropores visible in S950C90 after dye **1** adsorption compared to the image of S950C90 before dye **1** adsorption. This supports the incorporation of dye molecules within the porous structure of S950C90. The main elemental compositions of S950C90 shown by the EDS mapping are oxygen and sulphur. After methylene blue adsorption, EDS analysis showed the additional presence of nitrogen and chlorine and the presence of significantly more sulphur on the surface of S950C90.

3.3. Correlation of methylene blue adsorption with starbon® textural properties

The eleven materials used in this work had a wide range of textural properties (Table 1), methylene blue saturated adsorption capacities (Table 2), Gibbs free energies of adsorption (Table 3) and initial rates of adsorption (h$_2$ in Table 4). This allowed correlations between the textural properties and the dye **1** adsorption parameters to be
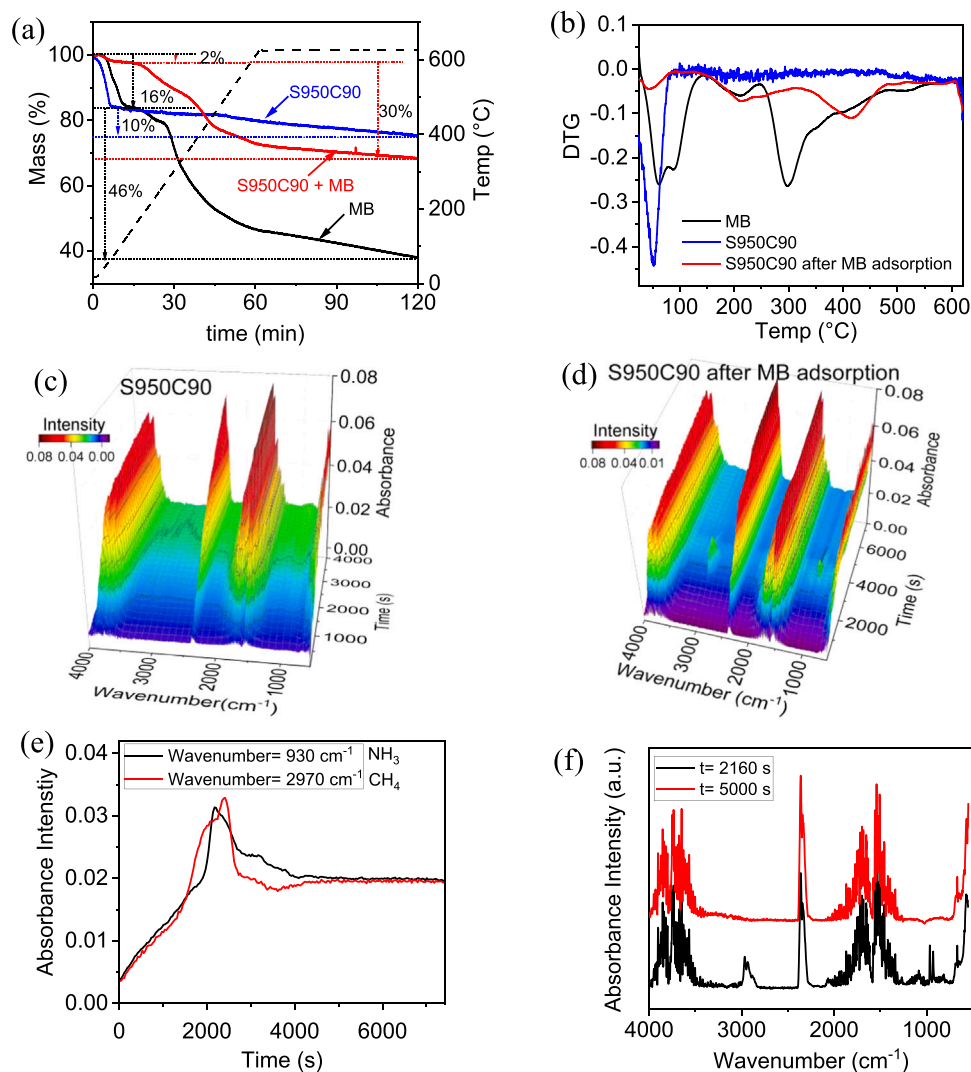
Fig. 6. (a) TGA and (b) DTG curves from the pyrolysis under nitrogen of methylene blue (MB) and S950C90 before and after methylene blue adsorption; (c,d) real-time FTIR spectra of the off-gases from the pyrolysis of S950C90 before (c) and after (d) methylene blue adsorption; (e) change of absorbance with time of the FTIR peaks corresponding to ammonia and methane; and (f) FTIR spectra at 2160 s (black) and 5000 s (red) during the pyrolysis of S950C90 after methylene blue adsorption.

Table 5
Combustion analysis and XPS data for S950C90 and S800K4, before and after adsorption of dye **1**.

Material	Combustion analysis					XPS analysis			
	C (%)	H (%)	N (%)	S (%)	Rest (%)	C (%)	O (%)	N (%)	S (%)
S950C90	88.7	0	0	1.2	10.1	98.5	1.3	0	0.1
S950C90 + **1**	77.1	3.4	4.3	4.3	10.9	91.3	3.1	3.5	1.7
S800K4	78.3	0	0	1.7	20.0	88.2	10.6	0.4	0.2
S800K4 + **1**	74.2	3.3	4.9	4.0	13.7	78.1	11.9	5.4	2.7

investigated (see supporting information). Nine textural properties were studied[2] and whilst no correlations were found between these and the Gibbs free energies of adsorption or the initial rates of adsorption, both the BET surface area and the micropore volume showed a strong linear correlation (R^2 = 0.91 and 0.92 respectively) with the saturated

methylene blue adsorption capacity (Fig. 10).[3]

Since dye **1** has a width of 0.72 nm (Fig. 1), it cannot fit into micropores with a diameter less than 0.7 nm. Therefore, the correlation of methylene blue saturated adsorption capacity with ultramicropore

---

[2] The textural properties investigated were: micropore surface area, external surface area, BET surface area, micropore volume, mesopore volume, total pore volume, ratio of micropore volume to total pore volume, ratio of mesopore volume to total pore volume and ratio of micropore volume to mesopore volume.

[3] A single plot of methylene blue adsorption capacity against the product of BET surface area and micropore volume also gave a good correlation (R^2 = 0.89), though this was lower than the correlations seen for the plots against the two parameters individually (see supporting information). S800K5 is an outlier in this plot and when it is removed, the goodness of fit increases to R^2 = 0.96 which is comparable to the two individual plots.
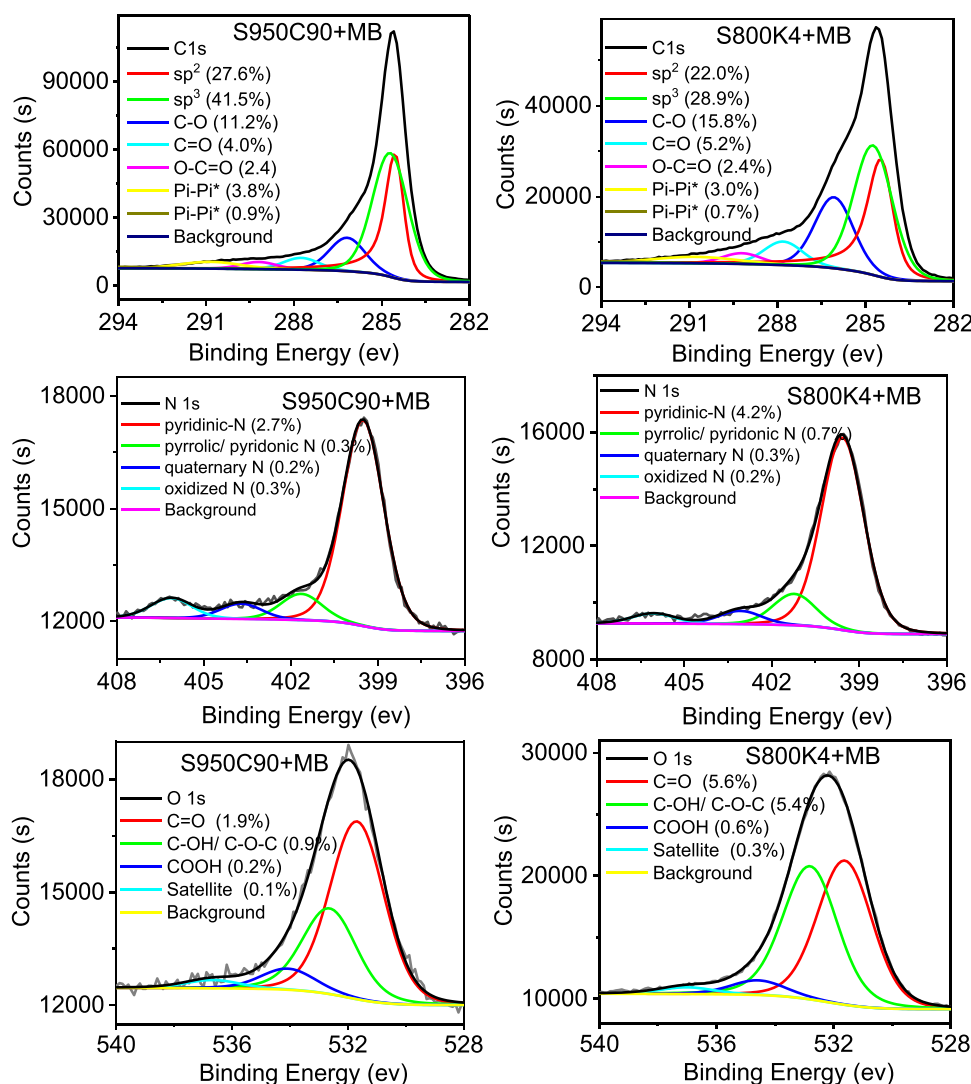
Fig. 7. High-resolution C1s (top), N1s (middle) and O1s (bottom) spectra of S950C90 (left) and S800K4 (right) after dye **1** adsorption. MB = methylene blue.
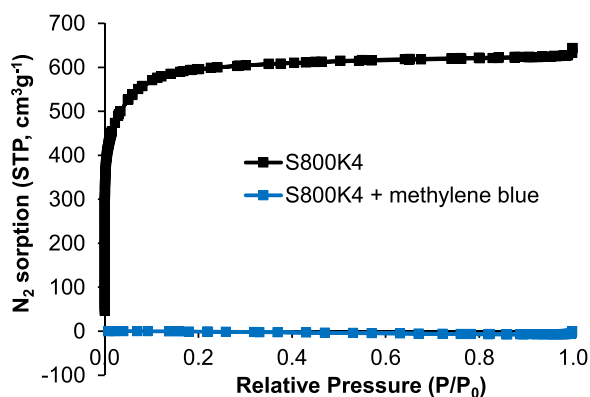
Fig. 8. N₂ sorption isotherms at 77 K of S800K4 before (black) and after (blue) adsorption of methylene blue.

volume (volume of pores with a diameter less than 0.7 nm) (Zdravkov et al., 2007) and supramicropore volume (volume of pores with a diameter of 0.7–2.0 nm) (Zdravkov et al., 2007) was also investigated (see supporting information). As expected the correlation with ultra-micropore volume ($R^2 = 0.77$) was weaker than that with supra-micropore volume ($R^2 = 0.89$). However, the best fit was still with the total micropore volume. For mesopores (diameter of 2–50 nm), the correlation between dye **1** adsorption capacity and pore volume vanishes ($R^2 = 0.002$) as the dye molecules can easily enter and leave the pores (Ge and Liu, 2016). The importance of micropore size is shown by comparison of the dye **1** saturated adsorption capacities of S800K4 and S800K5 (Table 2). S800K5 exhibits a lower saturated adsorption capacity than S800K4, even though its BET surface area and micropore volume are higher than those of S800K4 (Table 1). However, more of the micropores in S800K5 are ultramicropores than in S800K4. Hence, S800K5 has a slightly lower supramicropore volume than S800K4 and thus has a lower volume of micropores that are accessible to dye **1**. S800K5 is an outlier in both correlations shown in Fig. 10 and when it is removed, the correlations improve further ($R^2 = 0.96$ and 0.97).

The mesopore volume of the Starbon® materials does have a beneficial impact on their methylene blue saturated adsorption capacities as seen by comparison of the data for S800K1 with S800K2 and for S800K5 with S950C90 (Tables 1 and 2). Due to its higher mesopore volume, the saturated adsorption capacity of S800K1 is higher than that of S800K2, although its surface area and micropore volume are both slightly lower. Similarly, the surface area and micropore volume of S800K5 and S950C90 are very similar, whereas, due to its additional mesopore volume, the saturated adsorption capacity of S950C90 is particularly high. The absence of a direct correlation between methylene blue saturated adsorption capacity and mesopore volume suggests that the

(a)

(b)
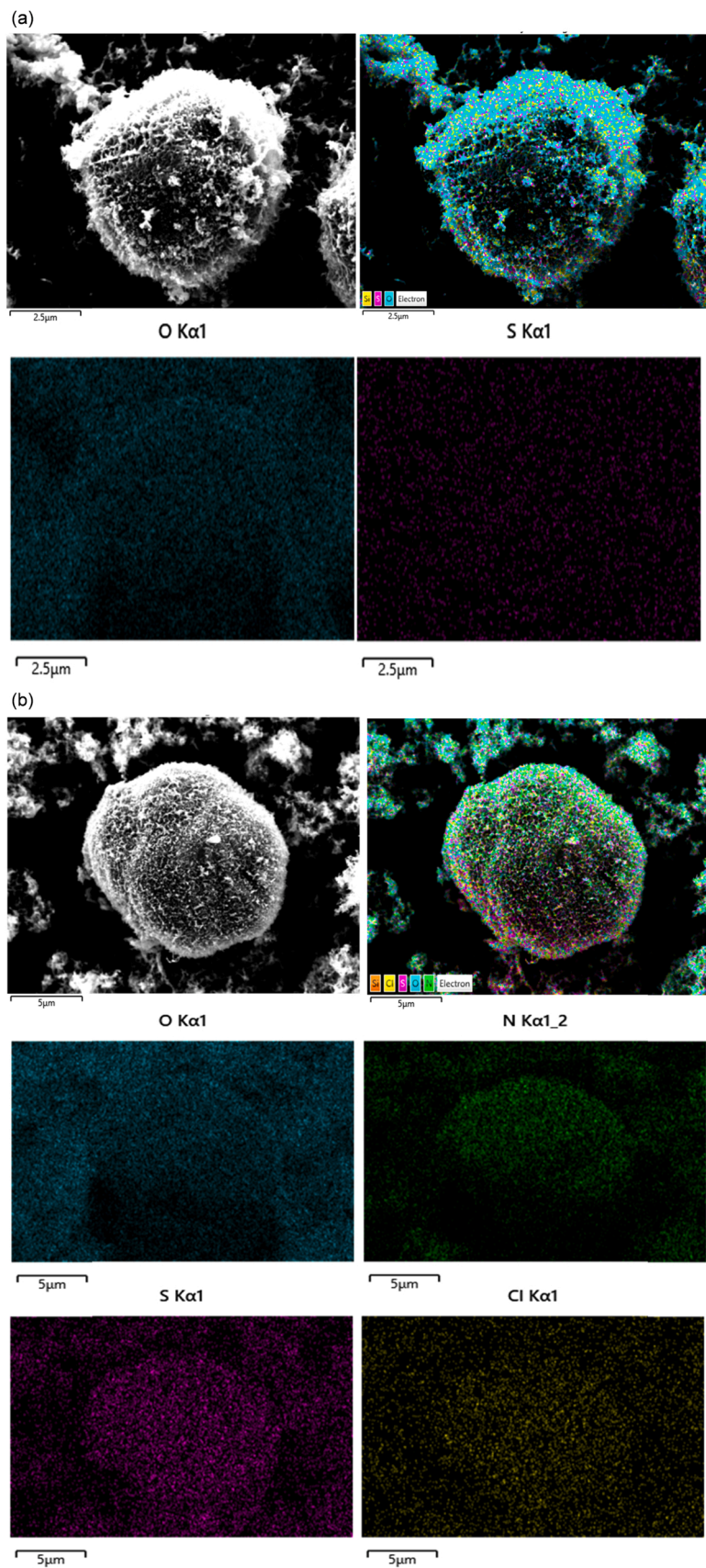
Fig. 9. SEM-EDS images of (a) S950C90 and (b) S950C90 after methylene blue adsorption.
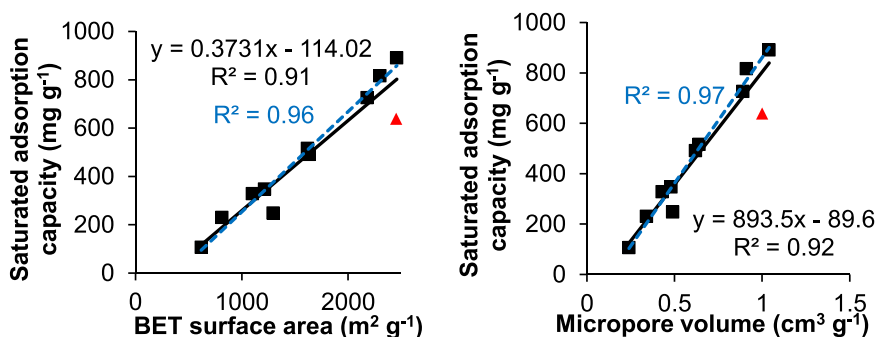
Fig. 10. Correlation of saturated adsorption capacity for methylene blue at 298 K with BET surface area and micropore volume. S800K5 is shown by the red triangle and is not included in the blue trend lines.

role of the mesopores is to enhance the access of dye **1** to supra-micropores within the structure of the adsorbent. Overall, the correlation analysis indicates that to maximise the methylene blue saturated adsorption capacity of a material, the BET surface area and micropore volume of the adsorbent should both be as high as possible. A high mesopore volume will also be beneficial for increasing the rate of adsorption.

3.4. Adsorption of other dyes by S950C90

3.4.1. Methyl orange and phenol red

To explore the generality of dye adsorption by activated Starbons®, the most active adsorbent for methylene blue **1** (S950C90) was also tested as an adsorbent for methyl orange **2** (Saeed et al., 2022) and phenol red **3** (Nanthamathee and Dechatiwongse, 2021). These dyes were chosen since whilst methylene blue **1** is a cationic heteroaromatic dye, methyl orange is an anionic azo-dye and phenol red is a neutral triarylmethyl dye. Fig. 11 shows the equilibrium adsorption capacities and removal efficiencies obtained for each of dyes **1–3** at 298 K with an initial dye concentration of 500 mg L^{-1}. There was no significant difference between the adsorption capacities (797–826 mg g^{-1}) or removal efficiencies (80–83%) between the three dyes, indicating that S950C90 is a highly effective adsorbent for dyes, irrespective of their chemical structure or charge.

The saturated adsorption capacities of dyes **2** and **3** onto S950C90 significantly exceed the reported saturated adsorption capacities of these dyes onto other materials. Methyl orange **2** has reported saturated adsorption capacities of: 111 mg g^{-1} onto active carbon prepared from grape seed (Yönten et al., 2020); 162 mg g^{-1} for sodium hydroxide activated carbon prepared from boiler residue (Martini et al., 2018); and 338 mg g^{-1} for waste cellulose-derived porous carbon (Sun et al., 2019). Reported phenol red **3** saturated adsorption capacities are: 56 mg g^{-1} onto titanium oxide nanoparticles loaded on activated carbon prepared from watermelon rind (Masoudian, . et al., 2019); 227 mg g^{-1} onto iron nanoparticles prepared from tea waste (Gautam et al., 2018); and

345 mg g^{-1} onto surfactant-modified clay (Gamoudi and Srasra, 2019).

3.4.2. Adsorption of dyes from simulated wastewater

To study the ability of S950C90 to purify realistic printing and dye effluent, the methodology of Tang et al. was adopted (Tang et al., 2021). Thus, two solutions (A and B) each containing six dyes (**1**, **2**, **4–7** Fig. 12) and four inorganic salts were prepared as detailed in Table 6. The decolourisation of solutions A and B upon treatment with S950C90 (0.5 mg mL^{-1}) for both 5 min and 4 h was then determined by integrating the UV–visible adsorption spectra (234–800 nm) of the mixtures before and after adsorption of the dyes (data in supporting information). The results are summarised in Fig. 13.

S950C90 was found to be highly effective at removing all six dyes from the simulated effluent. For the higher concentration effluent (A), 91 ± 4% of the dye was removed after a contact time of just five minutes, rising to 98.7 ± 0.2% after a contact time of four hours. With the lower concentration effluent (B), 93 ± 7% of the dye was removed after a contact time of five minutes and 99.7 ± 0.3% was removed after a contact time of four hours. The results suggest that competitive adsorption of inorganic ions or other dyes has no negative effect on the effectiveness of dye removal by S950C90. Simulated dye effluents A and B contain high concentrations of dyes and salts (Tang et al., 2021), so the virtually complete dye removal achieved by S950C90 indicates that it would be highly effective for industrial wastewater treatment, especially when compared with other adsorbents reported in the literature (Machado et al., 2012; Ribas et al., 2020; Tang et al., 2021; Grassi et al., 2021).

3.5. Comparison of methylene blue saturated adsorption capacities by activated Starbons® and other biomass derived carbons

Table 7 compares the methylene blue saturated adsorption capacity of S800K4 and S950C90 with those of 17 other biomass derived carbonaceous materials. The adsorption capacities of S950C90 are amongst the highest values reported. Only sodium hydroxide activated
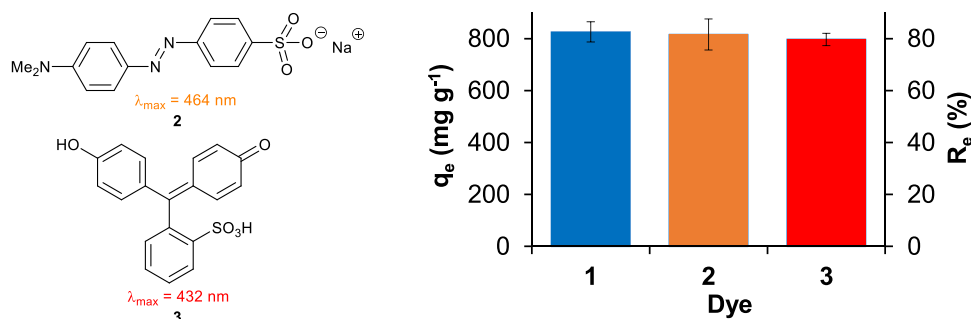
Fig. 11. Structures of methyl orange **2** and phenol red **3** and the adsorption capacity of S950C90 for each of dyes **1–3** at 298 K with $C_0 = 500$ mg L^{-1}. Adsorption measurements were made after 4 and 24 h to ensure that equilibrium had been reached. Error bars represent one standard deviation.

λ_{max} = 426 nm
4

λ_{max} = 651 nm
7

λ_{max} = 509 nm
5

λ_{max} = 625 nm
6
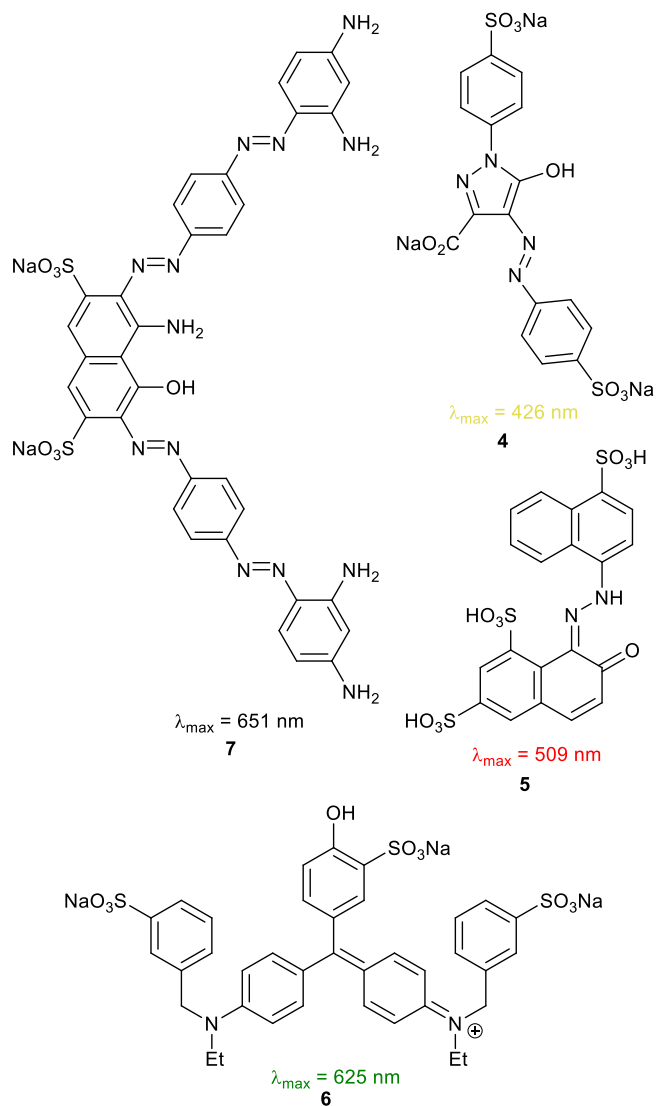
Fig. 12. Structures of lemon yellow **4**, acid red 18 **5**, direct fast green **6** and direct fast black **7**.

Table 6
Composition of the simulated dye effluents.

Dye/salt	Effluent A (mg L^{-1})[a]	Effluent B (mg L^{-1})[a]
Methylene blue **1**	200	120
Methyl orange **2**	50	30
Lemon yellow **4**	50	30
Acid red 18 **5**	100	60
Direct fast green **6**	50	30
Direct fast black **7**	50	30
NaCl	50	30
Na$_2$CO$_3$	50	30
NH$_4$Cl	50	30
Na$_2$SO$_4$	50	30

[a] The pH of the effluents were not adjusted.

coconut shell derived carbon has a similar adsorption capacity. However, activation using carbon dioxide is preferred as it is more sustainable and generates far less waste than activation using alkali metal hydroxides. These results suggest that S950C90 is a highly promising adsorbent for the purification of contaminated water (Manohara et al., 2021) and could contribute to achieving the key targets of UN sustainable development goal 6 (clean water and sanitation) (United Nations, 2022).
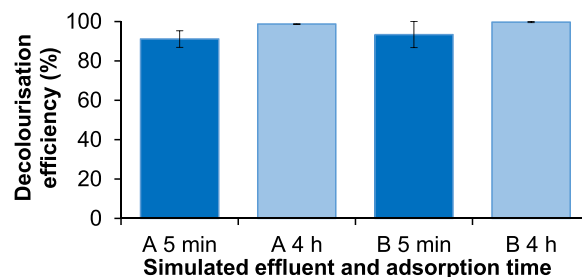
Fig. 13. Efficiency of decolourisation of simulated dye effluents A and B (see Table 6) by S950C90 after 5 min and 4 h. Error bars represent one standard deviation.

Table 7
Comparison of methylene blue adsorption using S800K4, S950C90 and other biomass derived carbonaceous materials.

Biomass precursor	Activation method	S$_{BET}$ (m^2 g^{-1})	Adsorption T (°C)	q$_e$ (mg g^{-1})	Reference
Bituminous coal	Steam	857	20	580[a]	El Qada et al. (2006)
Anaerobic granular sludge	ZnCl$_2$	741	25	91	Shi et al. (2014)
Sewage sludge and coconut shell	KOH	874	30 / 40	589[b] / 623[b]	Tu et al. (2021)
Coconut shell	NaOH	876	30	200	Islam et al. (2017)
Coconut shell	NaOH	2825	25	916	Cazetta et al. (2011)
Coconut shell	CO$_2$	1652	25	526	Jain et al. (2014)
Hazelnut shells	KOH	1700	20	524	Unur (2013)
Cashew nutshell	ZnCl$_2$	1871	25	476	Spagnoli et al. (2017)
Acacia mangium wood	H$_3$PO$_4$	1161	27	160	Danish et al. (2018)
Spruce-pine-fir	O$_2$	725	25	269	Chen et al. (2017)
Reed	K$_2$CO$_3$	1000	30	704	Zhou et al. (2017)
Lignin and chitosan	none	nr	20	36	Albadarin et al. (2017)
Mangrove fruit	KOH	1062	25	667	Sherugar et al. (2022)
Tomato waste	ZnCl$_2$	1093	30	400	Sayğili and Güzel (2016)
D-Fructose	none	431	20	83	Alatalo et al. (2016)
Sucrose	CO$_2$	1012	nr	211	Bedin et al. (2018)
Alginic acid	none	280	nr	186	Parker et al. (2012)
Starch (S800K4)	KOH	2299	25 / 35	817 / 845	This work
Starch (S950C90)	CO$_2$	2457	25 / 45	891, 937[b]/ 919	This work

nr = not reported.
[a] at pH 11;
[b] at pH 9.

4. Experimental

4.1. Materials

Unactivated S300 and S800 were prepared by the previously

reported freeze drying method (Borisova et al., 2015) and were activated using KOH, CO_2 or O_2 as previously described (Li et al., 2022). Methylene blue (1, high purity, biological stain) was supplied by Alfa Aesar; methyl orange 2, phenol red 3, lemon yellow 4, acid red 18 5 and direct fast green 6 were supplied by SigmaAldrich; direct fast black 7 was supplied by carbosynth; and water was deionized.

4.2. Instrumentation

Porosimetry was carried out by measuring nitrogen adsorption-desorption isotherms on a Micromeritics ASAP 2020 volumetric adsorption analyser at 77 K. Before analysis, powdered samples (~0.1 g) were degassed at 200 °C for 8 h. The BET surface area (Brunauer et al., 1938) was calculated from the nitrogen adsorption data at a relative pressure range of 0.01–0.2; the total pore volume was estimated at a relative pressure of 0.99; the BJH method (Thommes, 2010) was used for determination of mesopore volume and mesopore size distribution. The HK method for carbon materials with slit-shaped pores (Horvath and Kawazoe, 1983) was used for the determination of micropore volume, ultramicropore volume and micropore size distribution.

UV–visible spectra were recorded between 200 and 800 nm using a Thermo Genesys 180 UV–visible spectrometer. Distilled water was used as reference. Standard dye solutions of known concentrations (1–14 mg L^{-1}) were prepared and analysed to produce calibration curves (see supporting information) based on the adsorption at λ_{max} = 665, 464 or 432 nm for dyes 1–3 respectively. These curves were then used to determine the concentration of dye remaining in solutions. The Zeta potential of samples was determined by using a Malvern Zetasizer Nano ZS90 instrument. Sample (1 mg) was added to distilled water (20 mL) and the pH of the mixture was adjusted to 3–11 by adding hydrochloric acid (0.1 mol L^{-1}) or sodium hydroxide solution (0.1 mol L^{-1}) dropwise. A pH meter was used to measure the pH of the solutions. The solution was then sonicated for five minutes before analysis. TG-FTIR curves and spectra were recorded on a NETZSCH STA409 coupled to a Bruker Equinox 55 FTIR. Samples were heated from room temperature to 625 °C at a rate of 10 °C min^{-1} and then held at 625 °C for 1 h. The mass changes of samples as a function of temperature or time during thermal treatments were recorded by the STA409 whilst infrared spectra of gaseous decomposition products were recorded by the attached FTIR.

CHNS analysis was carried out by the University of York combustion analysis service using an Exeter Analytical Inc. CE-440 analyser and a high temperature combustion method. XPS analysis was performed by the UK national XPS service at the University of Cardiff using a Thermo K-Alpha+ XPS fitted with a monochromated Al kα X-ray source. Data were collected at a pass energy of 2150 eV for survey spectra and 40 eV for high-resolution scans. The spectra were collected at a pressure below 10^{-7} Torr and a temperature of 294 K. Peaks were fit with a Shirley background prior to component analysis. Data was analysed using CasaXPS (v2.3.34) after subtraction of the background and using modified sensitivity factors as supplied.

SEM analysis was carried out using a JEOL 7800 F scanning electron microscope and a LED detector with an accelerating voltage of 5 kV and a working distance of 10 mm. Energy dispersive X-ray spectrometry (EDS) analysis was performed by setting the accelerating voltage to 15 kV. The sample was mounted on an aluminium plate and coated with carbon to increase conductivity prior to analysis.

4.3. Dye adsorption studies

Stock solutions of dyes 1–3 in water (1000 mg L^{-1}) were prepared and diluted to various concentrations (25–700) mg L^{-1} as required. Experiments were carried out in triplicate by mixing adsorbent (10 mg) with an aqueous solution of dye (20 mL) at a controlled temperature (298, 308 or 318 K) and agitation rate (100 rpm) in a Julabo SW22 incubator shaker. At appropriate time intervals, samples of the dye solution (1 mL) were withdrawn, filtered through a 0.45 μm membrane filter and diluted with distilled water and analysed by UV–Vis spectrophotometry at a wavelength of 665, 464 or 432 nm for dyes 1–3 respectively. For adsorption isotherm studies, adsorptions were measured after 24 h to ensure that they had reached equilibrium. The effect of pH on the adsorption of dye 1 onto S950C90 was studied using an initial dye concentration of 500 mg L^{-1}. The pH of this solution was adjusted (to pH 3.0–11.0) using 0.1 M sodium hydroxide or 0.1 M hydrochloric acid.

4.4. S950C90 recyclability study

The recyclability of S950C90 towards adsorption of methylene blue 1 was studied over four cycles (Fig. 5). Firstly, the adsorption of an aqueous solution of dye 1 (20 mL, 500 mg L^{-1}) onto S950C90 (10 mg) was conducted at 298 K without adjusting the pH of the solution. After reaching adsorption equilibrium (4 h), the adsorbent was separated by centrifugation and the remaining solution was analysed by UV–vis spectrophotometry to determine the quantity of dye 1 that had been adsorbed. Then, desorption was carried out by mixing the adsorbed sample with EtOH and AcOH (150 mL, 20:1, v-v) and ultrasonicating the suspension for 5 min. This washing process was repeated three times, then the solid was collected by centrifugation. The solvent was combined and analysed by UV–vis spectrophotometry to determine the quantity of dye 1 that had been desorbed. The solid (S950C90) was then used for the next adsorption and desorption cycle.

4.5. Adsorption of dyes from simulated wastewater

Adsorption of simulated dye effluent onto S950C90 was carried out in triplicate by mixing S950C90 (10 mg) with a simulated dye effluent (20 mL, see Table 6) at 298 K in a Julabo SW22 incubator shaker with an agitation rate of 100 rpm. The pH of the simulated effluent was not adjusted. UV–vis spectra (190–800 nm) of the simulated effluents were recorded before adsorption and after adsorption by S950C90 for 5 min and 4 h. The area under the absorption bands from 234 to 800 nm was used to quantify the dye removal efficiency from the simulated dye effluent.

5. Conclusions

In this work we have shown that activated Starbons® derived from waste biomass (starch) are excellent adsorbents for the physisorption of methylene blue 1 and other dyes. The optimal materials (S800K4 and S950C90) show dye 1 adsorption capacities of over 800 mg g^{-1} at 25 °C. These high adsorption capacities are combined with high initial rates of adsorption (h_2 = 8065 and 34,770 mg g^{-1} min^{-1} for S800K4 and S8950C90 respectively at an initial concentration of 400 mg L^{-1}). The adsorption of dye 1 is pH dependent and the dye can be desorbed at pH 4 allowing the adsorbent to be reused.

The materials show excellent correlations between their dye 1 saturated adsorption capacities and both their BET surface areas and their micropore volumes. SEM-EDX analysis shows that dye 1 is adsorbed throughout the surface of the particles explaining the correlation with BET surface area. Porosimetry shows a complete loss of porosity after adsorption of dye 1, accounting for the correlation with micropore volume.

The optimal material (S950C90) was also studied as an adsorbent for methyl orange 2 and phenol red 3 and was found to have saturated adsorption capacities for these anionic and neutral dyes which were almost identical to that of the cationic dye methylene blue 1 (797–826 mg g^{-1}). In addition, the ability of S950C90 to decolourise simulated dye effluent composed of six dyes and four inorganic salts was studied and just 0.5 mg mL^{-1} of S950C90 was found to be sufficient to remove over 98.5% of the dyes present. These results indicate that S950C90 is a highly promising adsorbent for the purification of contaminated water which is essential to achieving UN sustainable

development goal 6 (clean water and sanitation) (United Nations, 2022).

CRediT authorship contribution statement

H. Li: Investigation; Conceptualization, Methodology, Writing – review & editing. **V. Budarin:** Methodology, Supervision. **James H. Clark:** Funding acquisition, Project administration, Resources, Supervision, Writing – review & editing. **M. North:** Funding acquisition, Project administration, Supervision, Writing – original draft. **X. Wu:** Methodology, Supervision.

Declaration of Competing Interest

The authors declare that they have no known competing financial interests or personal relationships that could have appeared to influence the work reported in this paper.

Acknowledgements

Appendix A. Supporting information

Supplementary data associated with this article can be found in the online version at doi:10.1016/j.jhazmat.2022.129174.

References

Adegoke, K.A., Bello, O.S., 2015. Dye sequestration using agricultural wastes as adsorbents. Water Resour. Ind. 12, 8–24. https://doi.org/10.1016/j.wri.2015.09.002.

Ahmed, S.F., Mofijur, M., Nuzhat, S., Chowdhury, A.T., Rafa, N., Uddin, M.A., Inayat, A., Mahlia, T.M.I., Ong, H.C., Chia, W.Y., Show, P.L., 2021. Recent developments in physical, biological, chemical, and hybrid treatment techniques for removing emerging contaminants from wastewater. J. Hazard. Mater. 416, 125912 https://doi.org/10.1016/j.jhazmat.2021.125912.

Al-Degs, Y., Khraisheh, M.A.M., Allen, S.J., Ahmad, M.N., 2000. Effect of carbon surface chemistry on the removal of reactive dyes from textile effluent. Water Res. 34, 927–935. https://doi.org/10.1016/S0043-1354(99)00200-6.

Al-Ghouti, M.A., Da'ana, D.A., 2020. Guidelines for the use and interpretation of adsorption isotherm models: A review. J. Hazard. Mater. 393, 122383 https://doi.org/10.1016/j.jhazmat.2020.122383.

Alam, S., Ullah, B., Khan, M.S., Khan, L., Shah, L.A., Zekker, I., Burlakovs, J., Kallistova, A., Pimenov, N., Yandri, E., Setyobudi, R.H., 2021. Adsorption kinetics and isotherm study of basic red 5 on synthesized silica monolith particles. Water 13, 2803. https://doi.org/10.3390/w13202803.

Alatalo, S.M., Makila, E., Repo, E., Heinonen, M., Salonen, J., Kukk, E., Sillanpaa, M., Titirici, M.M., 2016. Meso- and microporous soft templated hydrothermal carbons for dye removal from water. Green Chem. 18, 1137–1146. https://doi.org/10.1039/C5GC01796C.

Albadarin, A.B., Collins, M.N., Naushad, M., Shirazian, S., Walker, G., Mangwandi, C., 2017. Activated lignin-chitosan extruded blends for efficient adsorption of methylene blue. Chem. Eng. J. 307, 264–272. https://doi.org/10.1016/j.cej.2016.08.089.

Ali, H., 2010. Biodegradation of synthetic dyes—a review. Water Air Soil Pollut. 213, 251–273. https://doi.org/10.1007/s11270-010-0382-4.

Ani, J.U., Akpomie, K.G., Okoro, U.C., Aneke, L.E., Onukwuli, O.D., Ujam, O.T., 2020. Potentials of activated carbon produced from biomass materials for sequestration of dyes, heavy metals, and crude oil components from aqueous environment. Appl. Water Sci. 1–11. ⟨https://link.springer.com/article/10.1007/s13201-020-1149-8⟩.

Banat, I.M., Nigam, P., Singh, D., Marchant, R., 1996. Microbial decolorization of textile-dyecontaining effluents: a review. Bioresour. Technol. 58, 217–227. https://doi.org/10.1016/S0960-8524(96)00113-7.

Barton, S.S., 1987. The adsorption of methylene blue by active carbon. Carbon 25, 343–350. https://doi.org/10.1016/0008-6223(87)90005-4.

Bedin, K.C., Souza, I.P., Cazetta, A.L., Spessato, L., Ronix, A., Almeida, V.C., 2018. CO2-spherical activated carbon as a new adsorbent for Methylene Blue removal: Kinetic, equilibrium and thermodynamic studies. J. Mol. Liq. 269, 132–139. https://doi.org/10.1016/j.molliq.2018.08.020.

Bensalah, N., Alfaro, M.A.Q., Martinez-Huitle, C.A., 2009. Electrochemical treatment of synthetic wastewaters containing Alphazurine A dye. Chem. Eng. J. 149, 348–352. https://doi.org/10.1016/j.cej.2008.11.031.

Bhatnagar, A., Jain, A.K., 2005. A comparative adsorption study with different industrial wastes as adsorbents for the removal of cationic dyes from water. J. Colloid Interface Sci. 281, 49–55. https://doi.org/10.1016/j.jcis.2004.08.076.

Bhattacharyya, K.G., Sharma, 2004. Azadirachta indica leaf powder as an effective biosorbent for dyes: a case study with aqueous congo red solutions. J. Environ. Manag. 71, 217–229. https://doi.org/10.1016/j.jenvman.2004.03.002.

Borisova, A., De Bruyn, M., Budarin, V.L., Shuttleworth, P.S., Dodson, J.R., Segatto, M.L., Clark, J.H., 2015. A sustainable freeze-drying route to porous polysaccharides with tailored hierarchical meso- and macroporosity. Macromol. Rapid Commun. 36, 774–779. https://doi.org/10.1002/marc.201400680.

Brunauer, S., Emmett, P.H., Teller, E., 1938. Adsorption of gases in multimolecular layers. J. Am. Chem. Soc. 60, 309–319. https://doi.org/10.1021/ja01269a023.

Cazetta, A.L., Vargas, A.M., Nogami, E.M., Kunita, M.H., Guilherme, M.R., Martins, A.C., Silva, T.L., Moraes, J.C., Almeida, V.C., 2011. NaOH-activated carbon of high surface area produced from coconut shell: kinetics and equilibrium studies from the methylene blue adsorption. Chem. Eng. J. 174, 117–125. https://doi.org/10.1016/j.cej.2011.08.058.

Chaari, I., Moussi, B., Jamoussi, F., 2015. Interactions of the dye, C.I. direct orange 34 with natural clay. J. Alloy. Compd. 647, 720–727. https://doi.org/10.1016/j.jallcom.2015.06.142.

Chang, Z., Dai, J., Xie, A., He, J., Zhang, R., Tian, S., Yan, Y., Li, C., Xu, W., Shao, R., 2017. From lignin to three-dimensional interconnected hierarchically porous carbon with high surface area for fast and superhigh-efficiency adsorption of sulfamethazine. Ind. Eng. Chem. Res. 56, 9367–9375. https://doi.org/10.1021/acs.iecr.7b02312.

Chen, L., Ji, T., Brisbin, L., Zhu, J.H., 2015. Hierarchical porous and high surface area tubular carbon as dye adsorbent and capacitor electrode. ACS. Appl. Mater. Interfaces 7, 12230–12237. https://doi.org/10.1021/acsami.5b02697.

Chen, L., Ji, T., Mu, L., Shi, Y., Wang, H., Zhu, J., 2017. Pore size dependent molecular adsorption of cationic dye in biomass derived hierarchically porous carbon. J. Environ. Manag. 196, 168–177. https://doi.org/10.1016/j.jenvman.2017.03.013.

Danish, M., Ahmad, T., Hashim, R., Said, N., Akhtar, M.N., Mohamad-Saleh, J., Sulaiman, O., 2018. Comparison of surface properties of wood biomass activated carbons and their application against rhodamine B and methylene blue dye. Surf. Interfaces 11, 1–13. https://doi.org/10.1016/j.surfin.2018.02.001.

De Gisi, S., Lofrano, G., Grassi, M., Notarnicola, M., 2016. Characteristics and adsorption capacities of low-cost sorbents for wastewater treatment: a review. Sustain. Mater. Technol 9, 10–40. https://doi.org/10.1016/j.susmat.2016.06.002.

Dogan, M., Ozdemir, Y., Alkan, M., 2007. Adsorption kinetics and mechanism of cationic methyl violet and methylene blue dyes onto sepiolite. Dyes Pigments 75, 701–713. https://doi.org/10.1016/j.dyepig.2006.07.023.

El Qada, E.N., Allen, S.J., Walker, G.M., 2006. Adsorption of Methylene Blue onto activated carbon produced from steam activated bituminous coal: a study of equilibrium adsorption isotherm. Chem. Eng. J. 124, 103–110. https://doi.org/10.1016/j.cej.2006.08.015.

Fan, S.S., Wang, Y., Wang, Z., Tang, J., Tang, J., Li, X.D., 2017. Removal of methylene blue from aqueous solution by sewage sludge-derived biochar: adsorption kinetics, equilibrium, thermodynamics and mechanism. J. Environ. Chem. Eng. 5, 601–611. https://doi.org/10.1016/j.jece.2016.12.019.

Forgacs, E., Cserhati, T., Oros, G., 2004. Removal of synthetic dyes from wastewaters: a review. Environ. Int. 30, 953–971. https://doi.org/10.1016/j.envint.2004.02.001.

Fu, J.W., Xin, Q.Q., Wu, X.C., Chen, Z.H., Yan, Y., Liu, S.J., Wang, M.H., Xu, Q., 2016. Selective adsorption and separation of organic dyes from aqueous solution on polydopamine microspheres. J. Colloid Interface Sci. 461, 292–304. https://doi.org/10.1016/j.jcis.2015.09.017.

Gamoudi, S., Srasra, E., 2019. Adsorption of organic dyes by HDPy+-modified clay: effect of molecular structure on the adsorption. J. Mol. Struct. 1193, 522–531. https://doi.org/10.1016/j.molstruc.2019.05.055.

Gao, Q., Xu, J., Bu, X.H., 2019. Recent advances about metal–organic frameworks in the removal of pollutants from wastewater. Coord. Chem. Rev. 378, 17–31. https://doi.org/10.1016/j.ccr.2018.03.015.

Gautam, A., Rawat, S., Verma, L., Singh, J., Sikarwar, S., Yadav, B.C., Kalamdhad, A.S., 2018. Green synthesis of iron nanoparticle from extract of waste tea: an application for phenol red removal from aqueous solution. Environ. Nanotechnol. Monit. Manag. 10, 377–387. https://doi.org/10.1016/j.enmm.2018.08.003.

Gayathiri, M., Pulingam, T., Lee, K.T., Sudesh, K., 2022. Activated carbon from biomass waste precursors: Factors affecting production and adsorption mechanism. Chemosphere, 133764. https://doi.org/10.1016/j.chemosphere.2022.133764.

Ge, M.T., Liu, H.Z., 2016. A silsesquioxane-based thiophene-bridged hybrid nanoporous network as a highly efficient adsorbent for wastewater treatment. J. Mater. Chem. A 4, 16714–16722. https://doi.org/10.1039/C6TA06656A.

Golob, V., Ojstrsek, A., 2005. Removal of vat and disperse dyes from residual pad liquors. Dyes Pigments 64, 57–61. https://doi.org/10.1016/j.dyepig.2004.04.006.

González-García, P., 2018. Activated carbon from lignocellulosics precursors: a review of the synthesis methods, characterization techniques and applications. Renew. Sustain. Energy Rev. 82, 1393–1414. https://doi.org/10.1016/j.rser.2017.04.117.

Grassi, P., Drumm, F.C., Georgin, J., Franco, D.S.P., Dotto, G.L., Foletto, E.L., Jahn, S.L., 2021. Application of Cordia trichotoma sawdust as an effective biosorbent for removal of crystal violet from aqueous solution in batch system and fixed-bed column. Environ. Sci. Pollut. Res. 28, 6771–6783. https://doi.org/10.1007/s11356-020-11005-6.

Gürses, A., Doğar, Ç., Yalçın, M., Açıkyıldız, M., Bayrak, R., Karaca, S., 2006. The adsorption kinetics of the cationic dye, methylene blue, onto clay. J. Hazard. Mater. 131, 217–228. https://doi.org/10.1016/j.jhazmat.2005.09.036.

Hassan, M.M., Carr, C.M., 2021. Biomass-derived porous carbonaceous materials and their composites as adsorbents for cationic and anionic dyes: A review. Chemosphere 265, 129087. https://doi.org/10.1016/j.chemosphere.2020.129087.

Heidarinejad, Z., Rahmanian, O., Fazlzadeh, M., Heidari, M., 2018. Enhancement of methylene blue adsorption onto activated carbon prepared from Date Press Cake by

low frequency ultrasound. J. Mol. Liq. 264, 591–599. https://doi.org/10.1016/j.molliq.2018.05.100.

Horvath, G., Kawazoe, K., 1983. Method for the calculation of effective pore size distribution in molecular sieve carbon. J. Chem. Eng. Jpn. 16, 470–475. https://doi.org/10.1252/jcej.16.470.

Hu, X.S., Liang, R., Sun, G., 2018. Super-adsorbent hydrogel for removal of methylene blue dye from aqueous solution. J. Mater. Chem. A 6, 17612–17624. https://doi.org/10.1039/C8TA04722G.

Islam, M.A., Ahmed, M., Khanday, W., Asif, M., Hameed, B., 2017. Mesoporous activated coconut shell-derived hydrochar prepared via hydrothermal carbonization-NaOH activation for methylene blue adsorption. J. Environ. Manag. 2017 (203), 237–244. https://doi.org/10.1016/j.jenvman.2017.07.029.

Jain, A., Jayaraman, S., Balasubramanian, R., Srinivasan, M., 2014. Hydrothermal pre-treatment for mesoporous carbon synthesis: enhancement of chemical activation. J. Mater. Chem. A 2, 520–528. https://doi.org/10.1039/C3TA12648J.

Kabdasli, I., Tunay, O., Orhon, D., 1999. Wastewater control and management in a leather tanning district. Water Sci. Technol 40, 261–267. https://doi.org/10.2166/wst.1999.0055.

Khan, I., Saeed, K., Zekker, I., Zhang, B., Hendi, A.H., Ahmad, A., Ahmad, S., Zada, N., Ahmad, H., Shah, L.A., Shah, T., 2022. Review on methylene blue: its properties, uses, toxicity and photodegradation. Water 14, 242. https://doi.org/10.3390/w14020242.

Katheresan, V., Kansedo, J., Lau, S.Y., 2018. Efficiency of various recent wastewater dye removal methods: a review. J. Environ. Chem. Eng. 6, 4676–4697. https://doi.org/10.1016/j.jece.2018.06.060.

Kyzas, G.Z., Matis, K.A., 2015. Nanoadsorbents for pollutants removal: a review. J. Mol. Liq. 203, 159–168. https://doi.org/10.1016/j.molliq.2015.01.004.

Lee, J.W., Choi, S.P., Thiruvenkatachari, R., Shim, W.G., Moon, H., 2006. Evaluation of the performance of adsorption and coagulation processes for the maximum removal of reactive dyes. Dyes Pigments 69, 196–203. https://doi.org/10.1016/j.dyepig.2005.03.008.

Li, H., Li, C., Budarin, V.L., Clark, J.H., North, M., Wu, X., 2022. Synthesis, characterisation and carbon dioxide capture capacities of hierarchically porous Starbons®. Green Chem. 24, 1545–1560. https://doi.org/10.1039/D1GC03715C.

Li, X., Cui, Y.Y., Chen, Y.J., Yang, C.X., Yan, X.P., 2020. Facile synthesis of dual-functionalized microporous organic network for efficient removal of cationic dyes from water. Microporous Mesoporous Mater. 296, 110013 https://doi.org/10.1016/j.micromeso.2020.110013.

Machado, F.M., Bergmann, C.P., Lima, E.C., Royer, B., de Souza, F.E., Jauris, I.M., Calvete, T., Fagan, S.B., 2012. Adsorption of Reactive Blue 4 dye from water solutions by carbon nanotubes: experiment and theory. Phys. Chem. Chem. Phys. 14, 11139–11153. https://doi.org/10.1039/C2CP41475A.

Manohara, H.M., Nayak, S.S., Franklin, G., Nataraj, S.K., Mondal, D., 2021. Progress in marine derived renewable functional materials and biochar for sustainable water purification. Green Chem. 23, 8305–8331. https://doi.org/10.1039/D1GC03054J.

Martin, M.J., Artola, A., Balaguer, M.D., Rigola, M., 2003. Activated carbons developed from surplus sewage sludge for the removal of dyes from dilute aqueous solutions. Chem. Eng. J. 94, 231–239. https://doi.org/10.1016/S1385-8947(03)00054-8.

Martini, B.K., Daniel, T.G., Corazza, M.Z., de Carvalho, A.E., 2018. Methyl orange and tartrazine yellow adsorption on activated carbon prepared from boiler residue: kinetics, isotherms, thermodynamics studies and material characterization. J. Environ. Chem. Eng. 6, 6669–6679. https://doi.org/10.1016/j.jece.2018.10.013.

Mashkoor, F., Nasar, A., 2020. Magsorbents: potential candidates in wastewater treatment technology–a review on the removal of methylene blue dye. J. Magn. Magn. Mater. 500, 166408 https://doi.org/10.1016/j.jmmm.2020.166408.

Masoudian, N., Rajabi, M., Ghaedi, M., 2019. Titanium oxide nanoparticles loaded onto activated carbon prepared from bio-waste watermelon rind for the efficient ultrasonic-assisted adsorption of congo red and phenol red dyes from wastewaters. Polyhedron 173, 114105. https://doi.org/10.1016/j.poly.2019.114105.

Montoya-Suarez, S., Colpas-Castillo, F., Meza-Fuentes, E., Rodriguez-Ruiz, J., Fernandez-Maestre, R., 2016. Activated carbons from waste of oil-palm kernel shells, sawdust and tannery leather scraps and application to chromium(VI), phenol, and methylene blue dye adsorption. Water Sci. Technol. 73, 21–27. https://doi.org/10.2166/wst.2015.293.

Muhammad, I.J., Muhammad, A.N., 2007. Adsorption of dyes from aqueous solutions on activated charcoal. J. Hazard. Mater. 139, 57–66. https://doi.org/10.1016/j.jhazmat.2006.06.007.

Nanthamathee, C., Dechatiwongse, P., 2021. Kinetic and thermodynamic studies of neutral dye removal from water using zirconium metal-organic framework analogues. Mater. Chem. Phys. 258, 123924 https://doi.org/10.1016/j.matchemphys.2020.123924.

Ngulube, T., Gumbo, J.R., Masindi, V., Maity, A., 2017. An update on synthetic dyes adsorption onto clay based minerals: a state-of-art review. J. Environ. Manag. 191, 35–57. https://doi.org/10.1016/j.jenvman.2016.12.031.

Novais, R.M., Caetano, A.P., Seabra, M.P., Labrincha, J.A., Pullar, R.C., 2018. Extremely fast and efficient methylene blue adsorption using eco-friendly cork and paper waste-based activated carbon adsorbents. J. Clean. Prod. 197, 1137–1147. https://doi.org/10.1016/j.jclepro.2018.06.278.

O'Neill, C., Hawkes, F.R., Hawkes, D.L., Lourenco, N.D., Pinheiro, H.M., Delere, W., 1999. Colour in textile effluents – sources, measurement, discharge consents and simulation: a review. J. Chem. Technol. Biotechnol. 74, 1009–1018. https://doi.org/10.1002/(SICI)1097-4660(199911)74:11<1009::AID-JCTB153>3.0.CO;2-N.

Ozola-Davidane, R., Burlakovs, J., Tamm, T., Zeltkalne, S., Krauklis, A.E., Klavins, M., 2021. Bentonite-ionic liquid composites for Congo red removal from aqueous solutions. J. Mol. Liq. 337, 116373 https://doi.org/10.1016/j.molliq.2021.116373.

Parker, H.L., Hunt, A.J., Budarin, V.L., Shuttleworth, P.S., Miller, K.L., Clark, J.H., 2012. The importance of being porous: polysaccharide-derived mesoporous materials for use in dye adsorption. RSC Adv. 2, 8992–8997. https://doi.org/10.1039/C2RA21367B.

Plaza, M.G., Thurecht, K.J., Pevida, C., Rubiera, F., Pis, J.J., Snape, C.E., Drage, T.C., 2013. Influence of oxidation upon the CO_2 capture performance of a phenolic-resin-derived carbon. Fuel Process. Technol. 110, 53–60. https://doi.org/10.1016/j.fuproc.2013.01.011.

Qi, C.L., Xu, L.H., Zhang, M.X., Zhang, M., 2019. Fabrication and application of hierarchical porous carbon for the adsorption of bulky dyes. Microporous Mesoporous Mater. 290, 109651 https://doi.org/10.1016/j.micromeso.2019.109651.

Rad, L.R., Anbia, M., 2021. Zeolite-based composites for the adsorption of toxic matters from water: a review. J. Environ. Chem. Eng. 9, 106088 https://doi.org/10.1016/j.jece.2021.106088.

Rafatullah, M., Sulaiman, O., Hashim, R., Ahmad, A., 2010. Adsorption of methylene blue on low-cost adsorbents: A review. J. Hazard. Mater. 177, 70–80. https://doi.org/10.1016/j.jhazmat.2009.12.047.

Rahman, N.U., Ullah, I., Alam, S., Khan, M.S., Shah, L.A., Zekker, I., Burlakovs, J., Kallistova, A., Pimenov, N., Vincevica-Gaile, Z., Jani, Y., 2021. Activated ailanthus altissima sawdust as adsorbent for removal of acid yellow 29 from wastewater: kinetics approach. Water 13, 2136. https://doi.org/10.3390/w13152136.

Ramakrishna, K.R., Viraraghavan, T., 1997. Dye removal using low cost adsorbents. Water Sci. Technol 36, 189–196. https://doi.org/10.1016/S0273-1223(97)00387-9.

Rehman, A., Park, S.J., 2019. Tunable nitrogen-doped microporous carbons: Delineating the role of optimum pore size for enhanced CO_2 adsorption. Chem. Eng. J. 362, 731–742. https://doi.org/10.1016/j.cej.2019.01.063.

Ribas, M.C., De Franco, M.A., Adebayo, M.A., Lima, E.C., Parkes, G.M., Feris, L.A., 2020. Adsorption of Procion Red MX-5B dye from aqueous solution using homemade peach and commercial activated carbons. App. Water Sci. 10, 154. https://doi.org/10.1007/s13201-020-01237-9.

Robinson, T., McMullan, G., Marchant, R., Nigam, P., 2001. Remediation of dyes in textile effluent: a critical review on current treatment technologies with a proposed alternative. Bioresour. Technol. 77, 247–255. https://doi.org/10.1016/S0960-8524(00)00080-8.

Saeed, T., Naeem, A., Din, I.U., Farooq, M., Khan, I.W., Hamayun, M., Malik, T., 2022. Synthesis of chitosan composite of metal-organic framework for the adsorption of dyes; kinetic and thermodynamic approach. J. Hazard. Mater. 427, 127902 https://doi.org/10.1016/j.jhazmat.2021.127902.

Santoso, E., Ediati, R., Kusumawati, Y., Bahruji, H., Sulistiono, D.O., Prasetyoko, D., 2020. Review on recent advances of carbon based adsorbent for methylene blue removal from waste water. Mater. Today Chem. 16, 100233 https://doi.org/10.1016/j.mtchem.2019.100233.

Saravanan, A., Kumar, P.S., Jeevanantham, S., Karishma, S., Tajsabreen, B., Yaashikaa, P.R., Reshma, B., 2021. Effective water/wastewater treatment methodologies for toxic pollutants removal: processes and applications towards sustainable development. Chemosphere 280, 130595. https://doi.org/10.1016/j.chemosphere.2021.130595.

Saxena, R., Saxena, M., Lochab, A., 2020. Recent progress in nanomaterials for adsorptive removal of organic contaminants from wastewater. ChemistrySelect 5, 335–353. https://doi.org/10.1002/slct.201903542.

Saygılı, H., Güzel, F., 2016. High surface area mesoporous activated carbon from tomato processing solid waste by zinc chloride activation: process optimization, characterization and dyes adsorption. J. Clean. Prod. 113, 995–1004. https://doi.org/10.1016/j.jclepro.2015.12.055.

Sharma, S., Hasan, A., Kumar, N., Pandey, L.M., 2018. Removal of methylene blue dye from aqueous solution using immobilized Agrobacterium fabrum biomass along with iron oxide nanoparticles as biosorbent. Environ. Sci. Pollut. Res. 25, 21605–21615. ⟨https://link.springer.com/article/10.1007/s11356-018-2280-z⟩.

Sherugar, P., Padaki, M., Naik, N.S., George, S.D., Murthy, D.H., 2022. Biomass-derived versatile activated carbon removes both heavy metals and dye molecules from wastewater with near-unity efficiency: mechanism and kinetics. Chemosphere 287, 132085. https://doi.org/10.1016/j.chemosphere.2021.132085.

Shi, L., Zhang, G., Wei, D., Yan, T., Xue, X., Shi, S., Wei, Q., 2014. Preparation and utilization of anaerobic granular sludge-based biochar for the adsorption of methylene blue from aqueous solutions. J. Mol. Liq. 198, 334–340. https://doi.org/10.1016/j.molliq.2014.07.023.

Singh, A., Pal, D.B., Mohammad, A., Alhazmi, A., Haque, S., Yoon, T., Srivastava, N., Gupta, V.K., 2022. Biological remediation technologies for dyes and heavy metals in wastewater treatment: new insight. Bioresour. Technol. 343, 126154 https://doi.org/10.1016/j.biortech.2021.126154.

Singh, B.K., Rawat, N.S., 1994. Comparative sorption equilibrium studies of toxic phenols on flyash and impregnated flyash. J. Chem. Technol. Biotechnol. 61, 307–317. https://doi.org/10.1002/jctb.280610405.

Singh, K., Arora, S., 2011. Removal of synthetic textile dyes from wastewaters: a critical review on present treatment technologies. Crit. Rev. Environ. Sci. Technol. 41, 807–878. https://doi.org/10.1080/10643380903218376.

Singh, N.B., Nagpal, G., Agrawal, S., Rachna, 2018. Water purification by using adsorbents: a review. Environ. Technol. Innov. 11, 187–240. https://doi.org/10.1016/j.eti.2018.05.006.

Sokolowska-Gajda, J., Freeman, H.S., Reife, A., 1996. Synthetic dyes based on environmental considerations. Part 2: Iron complexes formazan dyes. Dyes Pigments 30, 1–20. https://doi.org/10.1016/0143-7208(95)00048-8.

Solangi, N.H., Kumar, J., Mazari, S.A., Ahmed, S., Fatima, N., Mubarak, N.M., 2021. Development of fruit waste derived bio-adsorbents for wastewater treatment: a review. J. Hazard. Mater. 416, 125848 https://doi.org/10.1016/j.jhazmat.2021.125848.

Spagnoli, A.A., Giannakoudakis, D.A., Bashkova, S., 2017. Adsorption of methylene blue on cashew nut shell based carbons activated with zinc chloride: the role of surface and structural parameters. J. Mol. Liq. 229, 465–471. https://doi.org/10.1016/j.molliq.2016.12.106.

Srinivasan, A., Viraraghavan, T., 2010. Decolorization of dye wastewaters by biosorbents: a review. J. Environ. Manag. 91, 1915–1929. https://doi.org/10.1016/j.jenvman.2010.05.003.

Subhan, H., Alam, S., Shah, L.A., Khattak, N.S., Zekker, I., 2022. Sodium alginate grafted hydrogel for adsorption of methylene green and use of the waste as an adsorbent for the separation of emulsified oil. J. Water Process Eng. 46, 102546 https://doi.org/10.1016/j.jwpe.2021.102546.

Sun, B., Yuan, Y., Li, H., Li, X., Zhang, C., Guo, F., Liu, X., Wang, K., Zhao, X.S., 2019. Waste-cellulose-derived porous carbon adsorbents for methyl orange removal. Chem. Eng. J. 371, 55–63. https://doi.org/10.1016/j.cej.2019.04.031.

Sun, Q., Yang, L., 2003. The adsorption of basic dyes from aqueous solution on modified peat–resin particle. Water Res. 37, 1535–1544. https://doi.org/10.1016/S0043-1354(02)00520-1.

Tan, I.A.W., Hameed, B.H., Ahmad, A.L., 2007. Equilibrium and kinetic studies on basic dye adsorption by oil palmfibre activated carbon. Chem. Eng. J. 127, 111–119. https://doi.org/10.1016/j.cej.2006.09.010.

Tan, X.F., Liu, S.B., Liu, Y.G., Gu, Y.L., Zeng, G.M., Hua, X.J., Wang, X., Liu, S.H., Jiang, L.H., 2017. Biochar as potential sustainable precursors for activated carbon production: Multiple applications in environmental protection and energy storage. Bioresour. Technol. 227, 359–372. https://doi.org/10.1016/j.biortech.2016.12.083.

Tang, X., Ran, G., Li, J., Zhang, Z., Xiang, C., 2021. Extremely efficient and rapidly adsorb methylene blue using porous adsorbent prepared from waste paper: Kinetics and equilibrium studies. J. Hazard. Mater. 402, 123579 https://doi.org/10.1016/j.jhazmat.2020.123579.

Thommes, M., 2010. Physical adsorption characterization of nanoporous materials. Chem-Ing-Tech 82, 1059–1073. https://doi.org/10.1002/cite.201000064.

Tran, T.H., Le, H.H., Pham, T.H., Nguyen, D.T., La, D.D., Chang, S.W., Lee, S.M., Chung, W.J., Nguyen, D.D., 2021. Comparative study on methylene blue adsorption behavior of coffee husk-derived activated carbon materials prepared using hydrothermal and soaking methods. J. Environ. Chem. Eng. 9, 105362 https://doi.org/10.1016/j.jece.2021.105362.

Tu, W., Liu, Y., Xie, Z., Chen, M., Ma, L., Du, G., Zhu, M., 2021. A novel activation-hydrochar via hydrothermal carbonization and KOH activation of sewage sludge and coconut shell for biomass wastes: Preparation, characterization and adsorption properties. J. Colloid Interface Sci. 593, 390–407. https://doi.org/10.1016/j.jcis.2021.02.133.

United Nations, 2022. ⟨https://www.un.org/sustainabledevelopment/water-and-sanitation/⟩ (accessed 02/03/2022).

Unur, E., 2013. Functional nanoporous carbons from hydrothermally treated biomass for environmental purification. Microporous Mesoporous Mater. 168, 92–101. https://doi.org/10.1016/j.micromeso.2012.09.027.

Walsh, G.E., Bahner, L.H., 1980. Toxicity of textile mill effluents to freshwater and estuarine algae, crustaceans and fishes. Environ. Pollut. Ser. A. 21, 169–179. https://doi.org/10.1016/0143-1471(80)90161-0.

Wang, Q., Lai, Z., Luo, C., Zhang, J., Cao, X., Liu, J., Mu, J., 2021. Honeycomb-like activated carbon with microporous nanosheets structure prepared from waste biomass cork for highly efficient dye wastewater treatment. J. Hazard. Mater. 416, 125896 https://doi.org/10.1016/j.jhazmat.2021.125896.

Wong, S., Ngadi, N., Inuwa, I.M., Hassan, O., 2018. Recent advances in applications of activated carbon from biowaste for wastewater treatment: a short review. J. Clean. Prod. 175, 361–375. https://doi.org/10.1016/j.jclepro.2017.12.059.

Wong, Y.C., Szeto, Y.S., Cheung, W.H., McKay, G., 2004. Adsorption of acid dyes on chitosan—equilibrium isotherm analyses. Process Biochem. 39, 693–702. https://doi.org/10.1016/S0032-9592(03)00152-3.

Wrobel, D., Boguta, A., Ion, R.M., 2001. Mixtures of synthetic organic dyes in a photoelectrochemical cell. J. Photochem. Photobiol. A Chem. 138, 7–22. https://doi.org/10.1016/S1010-6030(00)00377-4.

Xiao, F.S., Wang, L., Yin, C., Lin, K., Di, Y., Li, J., Xu, R., Su, D.S., Schlögl, R., Yokoi, T., Tatsumi, T., 2006. Catalytic properties of hierarchical mesoporous zeolites templated with a mixture of small organic ammonium salts and mesoscale cationic polymers. Angew. Chem. Int. Ed. 118, 3162–3165. https://doi.org/10.1002/anie.200600241.

Yagub, M.T., Sen, T.K., Afroze, S., Ang, H.M., 2014. Dye and its removal from aqueous solution by adsorption: a review. Adv. Colloid Interface Sci 209, 172–184. https://doi.org/10.1016/j.cis.2014.04.002.

Yönten, V., Sanyürek, N.K., Kivanç, M.R., 2020. A thermodynamic and kinetic approach to adsorption of methyl orange from aqueous solution using a low cost activated carbon prepared from Vitis vinifera L. Surf. Interfaces 20, 100529. https://doi.org/10.1016/j.surfin.2020.100529.

Zdravkov, B.D., Cermak, J.J., Sefara, M., Janku, J., 2007. Open Chem. 5, 385–395. https://doi.org/10.2478/s11532-007-0017-9.

Zhang, Y.L., Ji, G.Z., Li, C.J., Wang, X.X., Li, A.M., 2020. Templating synthesis of hierarchical porous carbon from heavy residue of tire pyrolysis oil for methylene blue removal. Chem. Eng. J. 390, 124398 https://doi.org/10.1016/j.cej.2020.124398.

Zhang, Z.Y., Xu, X.C., 2014. Wrapping carbon nanotubes with poly (sodium 4-styrene-sulfonate) for enhanced adsorption of methylene blue and its mechanism. Chem. Eng. J. 256, 85–92. https://doi.org/10.1016/j.cej.2014.06.020.

Zhou, L., Yu, Q., Cui, Y., Xie, F., Li, W., Li, Y., Chen, M., 2017. Adsorption properties of activated carbon from reed with a high adsorption capacity. Ecol. Eng. 102, 443–450. https://doi.org/10.1016/j.ecoleng.2017.02.036.